

p-NO₂-Bn-H₄neunpa and H₄neunpa-Trastuzumab: Bifunctional Chelator for Radiometal pharmaceuticals and ¹¹¹In Immuno-SPECT Imaging

Sarah Spreckelmeyer, Caterina F. Ramogida, Julie Rousseau, Karen Arane, Ivica Bratanovic, Nadine Colpo, Una Jermilova, Gemma Dias, Iulia Dude, Maria de Guadalupe Jaraquemada Peláez, Francois Benard, Paul Schaffer, and Chris Orvig

Bioconjugate Chem., **Just Accepted Manuscript** • DOI: 10.1021/acs.bioconjchem.7b00311 • Publication Date (Web): 06 Jul 2017

Downloaded from <http://pubs.acs.org> on July 19, 2017

Just Accepted

“Just Accepted” manuscripts have been peer-reviewed and accepted for publication. They are posted online prior to technical editing, formatting for publication and author proofing. The American Chemical Society provides “Just Accepted” as a free service to the research community to expedite the dissemination of scientific material as soon as possible after acceptance. “Just Accepted” manuscripts appear in full in PDF format accompanied by an HTML abstract. “Just Accepted” manuscripts have been fully peer reviewed, but should not be considered the official version of record. They are accessible to all readers and citable by the Digital Object Identifier (DOI®). “Just Accepted” is an optional service offered to authors. Therefore, the “Just Accepted” Web site may not include all articles that will be published in the journal. After a manuscript is technically edited and formatted, it will be removed from the “Just Accepted” Web site and published as an ASAP article. Note that technical editing may introduce minor changes to the manuscript text and/or graphics which could affect content, and all legal disclaimers and ethical guidelines that apply to the journal pertain. ACS cannot be held responsible for errors or consequences arising from the use of information contained in these “Just Accepted” manuscripts.

p-NO₂-Bn-H₄neunpa and H₄neunpa-Trastuzumab: Bifunctional Chelator for Radiometal pharmaceuticals and ¹¹¹In Immuno-SPECT Imaging

Sarah Spreckelmeyer,^{†,‡} Caterina F. Ramogida,[§] Julie Rousseau,[#] Karen Arane,[†] Ivica Bratanovic,[§] Nadine Colpo,[#] Una Jermilova,[§] Gemma M. Dias,[#] Iulia Dude,[#] Maria de Guadalupe Jaraquemada-Peláez,[†] François Bénard,[#] Paul Schaffer,[§] Chris Orvig^{†,*}

[†] Medicinal Inorganic Chemistry Group, Department of Chemistry, University of British Columbia, 2036 Main Mall, Vancouver, British Columbia, V6T 1Z1, Canada

[‡]Dept. Pharmacokinetics, Toxicology and Targeting, Research Institute of Pharmacy, University of Groningen, Antonius Deusinglaan 1, Groningen 9713 AV, The Netherlands

[§] Life Sciences Division, TRIUMF, 4004 Wesbrook Mall, Vancouver, British Columbia, V6T 2A3, Canada

[#] BC Cancer Agency, 675 West 10th Avenue, Vancouver, British Columbia, V5Z 1L3, Canada

* E-mail: orvig@ubc.chem.ca

Potentially nonadentate (N₅O₄) bifunctional chelator *p*-SCN-Bn-H₄neunpa and its immunoconjugate H₄neunpa-Trastuzumab for ¹¹¹In radiolabeling are synthesized. The ability of *p*-SCN-Bn-H₄neunpa and H₄neunpa-Trastuzumab to radiolabel quantitatively ¹¹¹InCl₃ at ambient temperature within 15 min or 30 min, respectively, is presented. Thermodynamic stability determination with In³⁺, Bi³⁺ and La³⁺ resulted in high pM values. In vitro human serum stability assays have demonstrated both ¹¹¹In complexes to have high stability over 5 days. Mouse biodistribution of [¹¹¹In][In(*p*-NO₂-Bn-neunpa)], compared to that of [¹¹¹In][In(*p*-NH₂-Bn-CHX-A"-DTPA)]²⁻, at 1 h, 4 h and 24 h shows fast clearance of both complexes from the mice within 24 h. In a second mouse biodistribution study, the immunoconjugates ¹¹¹In-neunpa-Trastuzumab and ¹¹¹In-CHX-A"-DTPA-Trastuzumab demonstrate a similar distribution profile, but with slightly lower tumor uptake of ¹¹¹In-neunpa-Trastuzumab compared to ¹¹¹In-CHX-A"-DTPA-Trastuzumab. These results were also confirmed by Immuno-SPECT imaging *in vivo*. These initial investigations reveal the acyclic bifunctional chelator *p*-SCN-Bn-H₄neunpa to be a promising chelator for ¹¹¹In (and other radiometals) with high in vitro stability, and also show H₄neunpa-Trastuzumab to be an excellent ¹¹¹In chelator, with promising biodistribution in mice.

Introduction

Early detection and specific therapy are the key factors for the successful treatment of cancer. ¹¹¹In (t_{1/2} = 2.8 days) and/or ¹⁷⁷Lu (t_{1/2} = 6.6 days) are important radioisotopes in nuclear medicine that match either the requirements for single photon emission tomography (SPECT) and performing dosimetry, or for therapeutic purposes, respectively. ¹¹¹In being a cyclotron-produced radiometal (via the ¹¹¹Cd(p,n)¹¹¹In reaction) emits gamma rays (245 and 171 keV) and Auger electrons. ¹⁷⁷Lu being a reactor-produced radiometal (¹⁷⁶Lu(n,γ)¹⁷⁷Lu) emits primarily beta particles (490 keV) that can be used for therapy.¹

A common method to incorporate metallic radioisotopes (i.e. radiometals) into radiopharmaceuticals is via chelation of the desired radioisotope using a bifunctional chelator (BFC). As implied by the name, BFCs possess two properties – they must chelate the radiometal of interest in a tight and stable metal-ligand complex, and the BFC must incorporate a point of attachment for conjugation to a targeting vector (e.g. biomolecule of interest in disease progression such as a peptide or antibody). Both macrocyclic and acyclic chelators are used in the clinic, and are also of interest in the field of medicinal inorganic chemistry research. The pros and cons of cyclic vs acyclic chelators are widely known and beyond debate.² Rele-

vant to ¹¹¹In and ¹⁷⁷Lu, macrocyclic DOTA (1,4,7,10-tetraazacyclododecane-1,4,7,10-tetraacetic acid) is the gold-standard chelator, while acyclic chelator DTPA (diethylenetriamine pentaacetic acid) and chiral analogue CHX-A"-DTPA are ubiquitous in ¹¹¹In radiopharmaceutical development (Figure 1). Recent studies developed bifunctional somatostatin analogues of DOTA with increased stability *in vivo*.³ As an acyclic gold-standard, the commercially available radiopharmaceutical OctreoScan (¹¹¹In-DTPA octeotide) reached approval in 1994 (Figure 1). Since the success of OctreoScan, several more bifunctional acyclic ¹¹¹In chelators that contain different biomolecules have been developed, hoping to overcome the limitations of OctreoScan. These include an increased physiological uptake which restricts the detection of small lesions, prolonged imaging protocol and relatively high radiation dose to the patients, as well as low image quality.⁴

Our group has developed several promising acyclic chelators for ¹¹¹In and/or ¹⁷⁷Lu, based on picolinic acid binding motifs, which we have since dubbed the “pa”-family of chelators.⁵⁻⁸ Of note, octadentate H₄octapa (N₄O₄) and its bifunctional analogue *p*-SCN-Bn-H₄octapa showed exceptional complexation properties (quantitative ¹¹¹In or ¹⁷⁷Lu radiolabeling in 10-30 minutes at ambient temperature) and favorable *in vivo* stability of resulting complexes.^{9,10} Furthermore, chiral ligands

$H_2CHXdedpa$ (N_4O_2) and $H_4CHXoctapa$ (N_4O_4) showed promising ^{68}Ga and ^{111}In radiolabeling properties, respectively, and subsequently impressive stability in human serum.⁸

Our group continues to design ligands that may incorporate large metal ions (such as radioactive actinides/lanthanides for imaging/therapy), which possess ideal properties for radiopharmaceutical incorporation, e.g. fast, mild, and quantitative complexation of radiometals at low ligand concentrations; formation of resultant thermodynamically stable and kinetically inert metal-complexes; and a convenient point of attachment to targeting vectors. Herein, we report the synthesis and characterization of a novel nonadentate (CN = 9) acyclic chelator $H_4neunpa$ (N_5O_4 , referred to herein as either $p-NO_2-Bn-H_4neunpa$ or $H_4neunpa$) and bifunctional analogue $p-SCN-Bn-H_4neunpa$ that was designed as a bifunctional analogue of $H_5decapa$ (N_5O_5), reported by our group in 2012.⁵ The carboxylic acid group on the middle nitrogen atom has been replaced by p -nitrobenzene-ethylene to keep its symmetry, and act as the bifunctional arm to attach the ligand to a biomolecule through a thiourea bond (Figure 1). We hypothesized that the extended diethylenetriamine backbone and nine coordinating atoms of $H_4neunpa$ may favorably form complexes with large metal ions such as In^{3+} (92 pm, CN = 8)¹¹, Lu^{3+} (103 pm, CN = 9), or Bi^{3+} (117 pm, CN = 8). Radiolabeling of ^{111}In and ^{177}Lu to $H_4neunpa$ was assessed and compared to gold-standards DOTA and CHX-A''-DTPA, and an *in vivo* biodistribution study of $H_4neunpa$ and CHX-A''-DTPA labeled with ^{111}In was performed. Thermodynamic stability constants of selected metal-*neunpa* complexes were also determined. Moreover, coupling of the HER2/*neu* targeting monoclonal antibody (mAb) Trastuzumab was performed via the reaction between the antibody's primary-amine(s) with the isothiocyanate functional group of $p-SCN-Bn-H_4neunpa$. The bioconjugate was labeled with ^{111}In , and *in vivo* biodistribution and SPECT/CT imaging studies were conducted and compared directly to a ^{111}In -CHX-A''-DTPA-Trastuzumab conjugate.

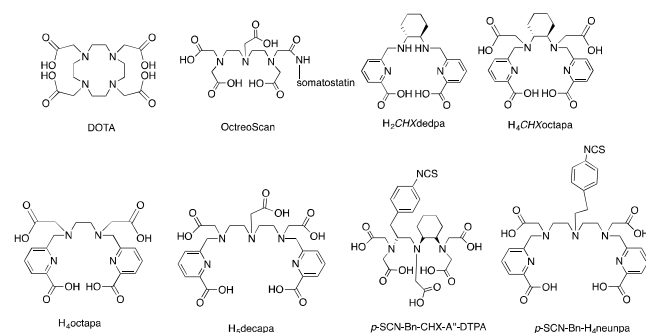


Figure 1. Structures of cyclic (DOTA) and acyclic (OctreoScan, CHX-A''-DTPA) commercial chelators, and acyclic “pa”-ligands $H_2CHXdedpa$, $H_4CHXoctapa$, $H_4octapa$, $H_5decapa$, and novel nonadentate chelator $p-SCN-Bn-H_4neunpa$ discussed in this work

Results and Discussion

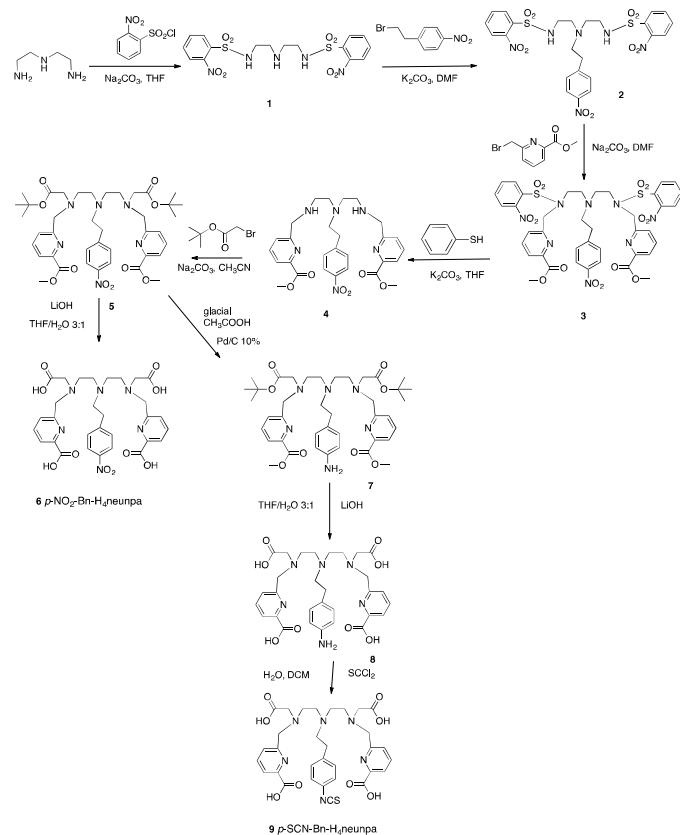
Synthesis and characterization of the ligand

The synthesis of the previously reported analogue $H_5decapa$ used N -benzyl protection, N -alkylation with an alkyl halide, benzyl deprotection via hydrogenation, a second alkyl halide N -alkylation, and finally deprotection in refluxing HCl (6M).¹⁰ The N -benzyl protection was found to be the yield-limiting step because the deprotection always resulted in partly eliminating the picolinic acid moieties. The use of O -nitrobenzenesulfonyl (nosyl) was found to give better cumulative yields compared to N -benzyl protection. Based on that, the bifunctional analogue $H_4neunpa$, was synthesized with a general reaction scheme that follows N -nosyl-protection, bifunctionalization on the middle nitrogen atom via N -alkylation, N -alkylation with picolinic acid, nosyl-deprotection with thiophenol, a second alkyl halide N -alkylation and ester-deprotection with LiOH to yield $p-NO_2-Bn-H_4neunpa$ **6** (Scheme 1). The isothiocyanate (NCS) analogue for mAb conjugation, $p-SCN-Bn-H_4neunpa$ **9**, was synthesized from the intermediate **5** followed by nitro-reduction, ester-deprotection with LiOH and isothiocyanate formation with thiophosgene (Scheme 1).

Starting from the diethylenetriamine backbone, the two primary amines were protected with the 2-nitrobenzenesulfonyl groups to yield compound **1**. Compound **1** is highly polar due to the two nosyl groups, thus a highly polar solvent like methanol is needed to separate it from the column. The second step is N -alkylation with 4-(2-bromoethyl)nitrobenzene. In order to maintain symmetry of the ligand, the ideal spot for bifunctionalization is the middle nitrogen. After that, N -alkylation with methyl-6-bromomethyl picolinate⁵ was performed to yield compound **3**. The most challenging step was the nosyl-deprotection, constantly resulting in low yields of compound **4**. The deprotected product is unfortunately highly polar and likely adsorbs on the surface of potassium carbonate, as seen by the red color of the salt. It was not possible to remove the large fractions of the deprotected product completely from the salt, which explains the low yield reported in the Experimental Section. Subsequently, alkyl halide N -alkylation was performed to yield product **5** with 71 % yield. $p-NO_2-Bn-H_4neunpa$ **6** was synthesized in a final step of ester deprotection with LiOH. This compound was further used for radiolabeling experiments as well as potentiometric stability titrations. The 1H NMR spectrum of the final product is shown in Figure 2.

$p-SCN-Bn-H_4neunpa$ **9** was synthesized starting from the intermediate **5** of the previous reaction route. Reduction of the nitro group with palladium on carbon yielded the amine-functionalized product **7**. The hydrolysis of the two *tert*-butyl esters and two methyl esters was performed differently from previous reports.^{5,12} Instead of acidic hydrolysis at high temperatures, compound **8** was synthesized by adding 10 eq. of lithium hydroxide to the reaction mixture at room temperature to yield the product, with a 50 % yield. The final step is the synthesis of the isothiocyanate-functionalized product **9**. This was achieved by the reaction of excess thiophosgene with the aromatic primary amine to yield the final product with a 59 % yield. Overall, the synthesis of $p-SCN-Bn-H_4neunpa$ from diethylenetriamine has a cumulative yield of 2.3 %, comparable to the overall synthesis yield of $H_5decapa$ (2.5 %).

Scheme 1. Synthetic scheme for *p*-SCN-Bn- H_4 neunpa and *p*-NO₂-Bn- H_4 neunpa



Synthesis and characterization of non-radioactive metal complexes

NMR

Three complexation experiments were performed with La³⁺, In³⁺ and Bi³⁺. ¹H NMR spectra of the *p*-NO₂-Bn- H_4 neunpa ligand precursor, and corresponding La and In complexes can be found in Figure 2. The [La(*p*-NO₂-Bn- H_4 neunpa)]⁺ complex shows ¹H NMR upfield shifts of the alkyl-region; this effect has been previously observed in our group.¹³ The aromatic region is more resolved and shows a splitting of the peaks. Integration of all peaks gives the same number of protons compared to the uncomplexed ligand. Furthermore, the HSQC spectra of this complex (Figure S2) shows the same number of carbons compared to the bare ligand, suggesting that there is only one isomer in solution. In contrast, the ¹H NMR spectrum of [In(*p*-NO₂-Bn- H_4 neunpa)]⁺ shows more splitting in the aromatic and alkyl regions. The aromatic peaks are sharp and well resolved and integrating the peaks suggests one major static isomer. In addition, the COSY spectrum of this complex shows clear coupling of several peaks in the complex alkyl region (Figure S12), leading to the assumption there are fluxional isomers in solution. Comparing these results to those with [In(decapa)]²⁺, which gave a complex ¹H NMR spectrum with multiple isomers presumably due to several unbound carboxylates¹⁰, we can see an improvement in terms of isomerization by replacing one carboxylate group with the functionalization arm on the middle nitrogen atom of the diethylenetriamine backbone. Due to insolubility of the Bi complex, the ¹H

NMR spectrum cannot be used for proper assignments (Figure S1).

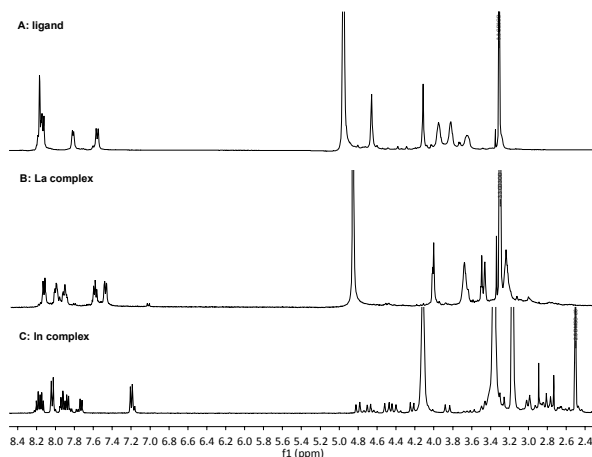


Figure 2. ¹H NMR spectra of A: *p*-NO₂-Bn- H_4 neunpa-*p*-Bn-NO₂ (400 MHz, CDCl₃, 25 °C); B: [La(*p*-NO₂-Bn- H_4 neunpa)]⁺ (400 MHz, CDCl₃, 25 °C); C: [In(*p*-NO₂-Bn- H_4 neunpa)]⁺ (400 MHz, DMSO-*d*₆, 25 °C)

IR

Due to the insolubility of [Bi(*p*-NO₂-Bn- H_4 neunpa)]⁺, an IR experiment on the solid was performed (Figure 3). Shifts of various peaks of the ligand itself compared to the Bi complex can be observed. The OH stretch at 2500 cm⁻¹ disappeared after complexation, suggesting that the carboxylic acids are bound to the metal ion; the carboxyl stretch at 1700 cm⁻¹ disappeared as well, supporting this assumption. The two stretches of the nitro functional group (1500 cm⁻¹ and 1400 cm⁻¹) stayed the same. The stretch at 1200 cm⁻¹ in the ligand spectra can be assigned as a C-N stretch that shifts to lower energies (1000 cm⁻¹) when bound to the metal ion.

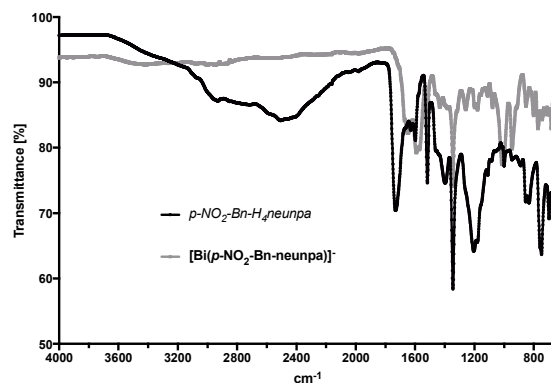


Figure 3. IR spectra of *p*-NO₂-Bn- H_4 neunpa and [Bi(*p*-NO₂-Bn- H_4 neunpa)]⁺

Thermodynamic Stability

The extended diethylenetriamine backbone, along with the nonadentate N₅O₄ binding motif of H_4 neunpa, were specifically designed to accommodate binding of larger metal ions. As such, the protonation constants of H_4 neunpa as well as the

stability constants of the respective La^{3+} , Bi^{3+} and In^{3+} complexes were determined at 25 °C in 0.16 M NaCl aqueous

solution. The stepwise protonation constants ($\log K$) obtained are presented in Table 1 together with protonation and

Table 1. Stepwise Protonation Constants ($\log K_{\text{HHL}}$) of H_4neunpa (25 °C, $I = 0.16$ M NaCl)^a

equilibrium reaction	neunpa ⁴⁻ (this work)	decapa ⁵⁻ (this work)	(this octapa ⁴⁻¹⁰)	DTPA ¹⁴	CHX-A''-DTPA ¹⁴	DOTA ¹⁵
$\text{L} + \text{H}^+ \rightleftharpoons \text{HL}$	10.92(2)	11.03(3)	8.59(4)	11.84	12.30	12.60(1)
$\text{HL} + \text{H}^+ \rightleftharpoons \text{H}_2\text{L}$	9.29(2)	9.20(3)	5.59(6)	9.40	9.24	9.70(1)
$\text{H}_2\text{L} + \text{H}^+ \rightleftharpoons \text{H}_3\text{L}$	6.79(2)	6.86(4)	3.77(2)	4.85	5.23	4.50(1)
$\text{H}_3\text{L} + \text{H}^+ \rightleftharpoons \text{H}_4\text{L}$	4.02(3)	4.43(4)	2.77(4)	3.10	3.32	4.14(1)
$\text{H}_4\text{L} + \text{H}^+ \rightleftharpoons \text{H}_5\text{L}$	2.97(2)	3.46(5)	2.79(4)	2.20	2.18	2.32(1)
$\text{H}_5\text{L} + \text{H}^+ \rightleftharpoons \text{H}_6\text{L}$	2.39(5)	2.84(6)	ND			
$\text{H}_6\text{L} + \text{H}^+ \rightleftharpoons \text{H}_7\text{L}$	ND	2.52(4)				
$\text{H}_7\text{L} + \text{H}^+ \rightleftharpoons \text{H}_8\text{L}$		ND				

^a Literature data of related systems are presented for comparison. L = Ligand and charges of ligand species and metal complexes were omitted for simplicity.

stability constants reported for the related ligands H_5decapa , H_4octapa , DTPA and CHX-A''-DTPA. A straightforward comparison of the ability of different ligands to coordinate a specific metal ion (rather than the thermodynamic stability constants alone), is the conditional stability constant or pM value. pM is defined as $(-\log [\text{M}^{n+}]_{\text{free}})$ and is calculated at specific conditions ($[\text{M}^{n+}] = 1 \mu\text{M}$, $[\text{L}^x] = 10 \mu\text{M}$, pH 7.4 and 25 °C), taking into consideration both metal-ligand association and ligand basicity. The protonation constants of the new synthesized ligand H_4neunpa were determined by potentiometric titrations at pH 1.8-11.5 and by combined potentiometric-spectrophotometric titrations^{16,17} over the pH range 2.5-11.5. In Figure S3 are shown the sets of spectra obtained as a function of pH, at 7.18×10^{-4} M ligand concentration. The first and second protonation processes occur at the two terminal amines of the diethylenetriamine backbone ($\log K_1 = 10.92(2)$ and $\log K_2 = 9.29(2)$), as suggested by the appearance of a single isosbestic point at 284 nm between pH 8.33 and 11.32 in the UV-potentiometric titration (Figure S3c). The third protonation process ($\log K_3 = 6.79(2)$) is assigned to the central nitrogen atom in the backbone and is supported by the appearance of an isosbestic point at 293 nm in the pH region between 5.39 and 8.33 (Figure S3b). The fourth and fifth protonation processes are attributed to the picolinate moieties^{13,18} ($\log K_4 = 4.02(3)$ and $\log K_5 = 2.97(2)$). The UV-potentiometric titration showed also in this case a single isosbestic point at 296 nm for these protonation processes (Figure S3a). The sixth protonation step is attributable to the carboxylic acid substituent ($\log K_6 = 2.39(5)$) and was calculated from potentiometric titrations. The value of $\log K_7$ could not be determined, as the value was below the threshold of the electrode (pH < 2). H_4neunpa , the bifunctional analogue of the previously reported H_5decapa (for which we correct here the protonation constants, Table 1) presents overall fairly similar protonation constants, although the fourth and fifth protonation processes attributed to the picolinate moieties differ by 0.41 and 0.49 units respectively.

The higher protonation constants in the case of H_5decapa could be attributed to the higher negative charge of the ligand. The speciation plots for H_4neunpa and H_5decapa are shown in Figure S4 in the Supporting Information.

Potentiometric titrations of H_4neunpa were carried out in the presence of La^{3+} , Bi^{3+} , and In^{3+} in order to determine the stability constants of the corresponding metal complexes. For lanthanum, combined potentiometric-spectrophotometric titrations demonstrated that the complexation started from pH 2, based on the distinctive features of the spectra compared to the electronic spectra of H_4neunpa (Figures S3 and S5). The thermodynamic stability of $[\text{La}(\text{neunpa})]^-$ was determined to be $\log K_{\text{ML}} = 19.81(4)$ and pM = 16. This value is close to the values obtained for $[\text{La}(\text{octapa})]^-$ $\log K_{\text{ML}} = 19.92(6)$ ¹⁹ and $[\text{La}(\text{DTPA})]^{2-}$ $\log K_{\text{ML}} = 19.48$ ²⁰. Similar to the free ligand, the deprotonation of the $[\text{La}(\text{H}_2\text{neunpa})]^+$ and $\text{La}(\text{Hneunpa})$ species is marked by the appearance of a single isosbestic point at 291 nm between the pH range 2.42-8.23 and suggests that the deprotonations occur at the two terminal amines of the diethylenetriamine backbone (Figure S5a). The $[\text{La}(\text{neunpa})]^-$ species further deprotonates presumably due to the deprotonation of a coordinated water molecule with pK 9.78 to form the monohydroxo complexes (Figure S5b). Species distribution diagrams for the lanthanum(III) complexes of H_4neunpa are plotted in Figure S6. The thermodynamic stability constant of the bismuth(III) complexes of H_4neunpa could not be determined by direct potentiometric titrations as this requires the knowledge of the concentration of the free and bound metal ion at equilibrium, and even at pH 2 the Bi(III) complex was already significantly formed. The ligand-ligand competition method using $\text{Na}_2\text{H}_2\text{EDTA}$ as a known competitor was used to yield the stability constants presented in Table 2 and speciation plots in Figure S7. Particularly high thermodynamic stability of $[\text{Bi}(\text{neunpa})]^-$ was found, $\log K_{\text{ML}} = 28.76(9)$ and pBi = 27. The thermodynamic stability constant of the $[\text{Bi}(\text{neunpa})]^-$ complex is lower than those of $[\text{Bi}(\text{DTPA})]^{2-}$

and $[\text{Bi}(\text{CHX-A-DTPA})]^{2-}$ complexes¹⁴ and lower than that for $[\text{Bi}(\text{DOTA})]^-$; however, it is interesting to note that

Table 2. Stepwise Stability Constants (log *K*) of H₄neunpa complexes with La³⁺, Bi³⁺ and In³⁺ ^a

equilibrium reaction	neunpa ⁴⁻	decapa ⁵⁻¹⁰	octapa ⁴⁻	DTPA	CHX-A''-DTPA	DOTA
La ³⁺ + L ⇌ LaL	19.81(4)		19.92(6) ¹⁹	19.48 ²⁰		22.0 ²¹
LaL + H ⁺ ⇌ LaHL	8.05(5)					
LaHL + H ⁺ ⇌ LaH ₂ L	3.28(6)					
LaLOH + H ⁺ ⇌ LaL	9.78(4)					
Bi ³⁺ + L ⇌ BiL	28.76(9)			35.2(4) ¹⁴	34.9(4) ¹⁴	30.3 ²²
BiL + H ⁺ ⇌ BiHL	10.26(5)					
BiHL + H ⁺ ⇌ BiH ₂ L	3.8(1)					
BiLOH + H ⁺ ⇌ BiL	10.57(7)					
In ³⁺ + L ⇌ InL	28.17(2)	27.56(5)	26.8(1) ¹⁰	29.0 ^{23,24}		23.9(1) ²⁴
InL + H ⁺ ⇌ InHL	5.07(2)	5.47(3)	2.9(2) ¹⁰			
InHL + H ⁺ ⇌ InH ₂ L	3.40(3)	2.73(6)				
InLOH + H ⁺ ⇌ InL	9.41(3)	9.83(7)				
pLa ³⁺	16		19.7			
pBi ³⁺	27					27 ²⁵
pIn ³⁺	23.6	23.1	26.5 ¹⁰	25.7 ¹⁰		18.8 ¹⁰

^a Literature data for related systems are presented for comparison. L = Ligand and charges of ligand species and metal complexes were omitted for simplicity.

H₄neunpa and DOTA have the same pBi³⁺ value of 27 (Table 2). Despite the high formation constant of $[\text{In}(\text{H}_2\text{neunpa})]^{2+}$ $\log K_{\text{MLH}_2} = 36.64(3)$, the system is well determined by direct potentiometric titration taking advantage of the indium-chloride competing species. The system as in the case of lanthanum(III) and bismuth(III) complexes containing MLH₂, MLH, ML and ML(OH) complex species (Figure S8) presented a high $\log K_{\text{ML}} = 28.17(2)$ and pM = 23.6, which is significantly higher than for DOTA (Table 2), slightly higher than for the previously reported H₅decapa, 2.1 pM units lower than for DTPA and 2.9 pM units lower than for $[\text{In}(\text{octapa})]^-$. To our knowledge thermodynamic formation constants of the $[\text{In}(\text{CHX-A''-DTPA})]^{2-}$ have not been yet reported. It is noteworthy that, as with other previously reported ligands¹⁰, the trend of the stability constants and pM values and the human serum stability data do not correlate well, and despite the higher pM values for $[\text{In}(\text{octapa})]^-$ species or $[\text{In}(\text{DTPA})]^{2-}$ vs $[\text{In}(\text{neunpa})]^{2-}$, $[\text{In}(\text{neunpa})]^{2-}$ showed an exceptional serum stability 97.8(1) % after one day, 5.5 units higher than the $[\text{In}(\text{octapa})]^-$ complex, 7.9 units higher than the $[\text{In}(\text{CHX-A''-DTPA})]^{2-}$ complex and 9.5 units higher than the $[\text{In}(\text{DTPA})]^{2-}$ complex.

Radiolabeling Experiments with Unmodified Chelators

The radiolabeling properties of ¹⁷⁷Lu and ¹¹¹In with H₄neunpa were investigated, and compared directly to results obtained for the gold-standards DOTA and CHX-A''-DTPA.

Initial radiolabeling experiments revealed that *p*-NO₂-Bn-H₄neunpa could quantitatively complex ¹¹¹In³⁺ (radiochemical yield, RCY > 99%) in 10 minutes at room temperature (RT), pH 4, at ligand concentrations of 10⁻⁴ M. Subsequently, concentration-dependent labeling was performed by decreasing the ligand concentration 10-fold while keeping the ¹¹¹In activity constant. Quantitative radiolabeling was achieved at ligand concentrations as low as 10⁻⁷ M (Figure 4), at 10 min and ambient temperature. At decreasing ligand concentrations of 10⁻⁸, 10⁻⁹, and 10⁻¹⁰ M, radiochemical yields gradually decreased to 71.1, 10.5, and 1.5%, respectively. These results demonstrate the ability of *p*-NO₂-Bn-H₄neunpa to rapidly and efficiently complex ¹¹¹In in high specific activities at ambient temperatures. H₄octapa showed similar radiolabeling efficiencies at 10⁻⁷ M, results at lower ligand concentrations are not reported.¹⁰ In sharp contrast to the two “pa” ligands is the macrocyclic gold-standard DOTA which is reported to require heating samples at 100°C for 30 minutes to achieve high radiochemical yields.¹⁰ The acyclic chelator CHX-A''-DTPA is a relatively recent addition to the list of potential ¹¹¹In chelators; in contrast to DOTA it can efficiently complex In³⁺ isotopes at ambient temperatures yet exhibits comparable *in vivo* stability

to DOTA conjugates^{2,26}, making it a more appealing chelator for radiolabeling of heat-sensitive biomolecules such as affibodies or antibodies.²⁷⁻³¹ Our initial ¹¹¹In radiolabeling studies with *p*-NH₂-Bn-CHX-A''-DTPA at ligand concentrations of 10⁻⁴ M corroborate the efficient and mild labeling of this ligand which yielded RCYs >99%; however, two evident peaks in the HPLC radio-chromatogram are observed – one major product at 8.6 min and a minor product at 8.0 min (Figure S10), with the ratio between the major and minor product being 7.7. The appearance of two distinct peaks in the radio-chromatogram may indicate the formation of distinct ¹¹¹In-chelate isomers. Contrary to H₄neunpa, at *p*-NH₂-Bn-CHX-A''-DTPA concentrations of 10⁻⁷ and 10⁻⁸ M, ¹¹¹In labeling yield decreased to 75.0 and 3.4%, respectively. The ratio of major to minor product in the HPLC radio-chromatogram also changed drastically at lower ligand concentrations, with the ratio being close to unity (0.95) for 10⁻⁷ M labeling.

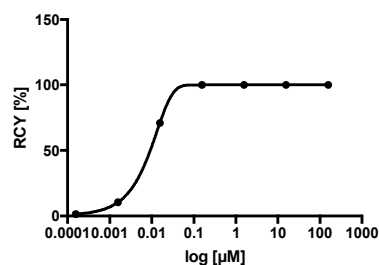


Figure 4. Radiolabeling results of ¹¹¹In-*p*-NO₂-Bn-neunpa (10min, RT, pH 4).

Unlike the facile labeling kinetics of [¹¹¹In(*p*-NO₂-Bn-neunpa)]⁻, initial radiolabeling studies with ¹⁷⁷Lu were unsuccessful. Attempted ¹⁷⁷Lu labeling at ligand concentrations of 10⁻⁴ M in 10 minutes at room temperature, pH 4 or 5.5, displayed a radiochemical yield of 12.4%; heating the sample to 40 °C for 1 hour did not improve RCY. Conversely, gold-standard DOTA was quantitatively radiolabeled (RCY > 99%) with ¹⁷⁷Lu when heated to 40 °C for 1 hour at the same ligand concentration (10⁻⁴ M). The inability of *p*-NO₂-Bn-H₄neunpa to complex ¹⁷⁷Lu isotopes at mild temperatures (< 40 °C) precluded further study with this isotope, since it was immediately obvious from the initial results that H₄neunpa was a poor match for ¹⁷⁷Lu and presented no potential advantage compared to the gold-standard DOTA.

Stability Studies with the Unmodified Chelators

In order to probe the kinetic inertness of the [¹¹¹In(*p*-NO₂-Bn-neunpa)]⁻ complex, a 5 d *in vitro* competition experiment was performed in the presence of human blood serum. Serum contains many endogenous ligands that can compete for In(III) binding *in vivo*, such as apo-transferrin and albumin, and any chelate-bound ¹¹¹In must therefore be sufficiently stable to withstand transchelation to such proteins. The *in vitro* stability of [¹¹¹In(*p*-NO₂-Bn-neunpa)]⁻ at 1 h, 1 and 5 d time points was tested alongside gold-standard [¹¹¹In(*p*-NH₂-Bn-CHX-A''-DTPA)]²⁻ for comparison (Table 3). The [¹¹¹In(*p*-NO₂-Bn-neunpa)]⁻ complex exhibited exceptional stability, remaining 97.8% intact over 5 days, while the [¹¹¹In(*p*-NH₂-Bn-CHX-A''-DTPA)]²⁻ complex showed an initial ~8% drop in stability after 1 h and subsequently stabilized for 5 days to remain

90.1% intact. The initial drop in stability after 1 h may be due to the presence of two isomers in the labeling reaction of *p*-NH₂-Bn-CHX-A''-DTPA (*vide supra*, major isomer 88.5% and minor isomer 11.5%). Studies with ⁸⁸Y-CHX-DTPA have demonstrated that thermodynamic stability of the resultant metal complex can be significantly affected by the absolute configuration, possibly due to unfavourable steric hindrance of certain stereoisomers;³² therefore, it is feasible that the minor isomer is kinetically labile with respect to transchelation to serum proteins. Indeed, [¹¹¹In(*p*-NO₂-Bn-neunpa)]⁻ displayed marginally higher stability than [¹¹¹In(*p*-NH₂-Bn-CHX-A''-DTPA)]²⁻, [¹¹¹In(DOTA)]⁻, and [¹¹¹In(octapa)]⁻ after 1 d (97.8 ± 0.1%, 89.9 ± 0.6, 88.3 ± 2.2%, 92.3 ± 0.04%, respectively).

Table 3. Human serum stability challenge data performed at 37°C (n = 3), with stability shown as percentage of intact ¹¹¹In-complex

Complex	1 h (%)	1 d (%)	5 d (%)
[¹¹¹ In(<i>p</i> -NO ₂ -Bn-neunpa)] ⁻	97.9 ± 0.3	97.8 ± 0.1	97.8 ± 0.7
[¹¹¹ In(<i>p</i> -NH ₂ -Bn-CHX-A''-DTPA)] ²⁻	91.8 ± 1.8	89.9 ± 0.6	90.1 ± 0.9
[¹¹¹ In(octapa)] ⁻ ^a	93.8 ± 3.6	92.3 ± 0.04	ND ^b
[¹¹¹ In(DOTA)] ⁻ ^a	89.6 ± 2.1	88.3 ± 2.2	ND ^b
¹¹¹ InCl ₃ (control) ^c	4.0	7.2	3.4

^aMouse serum stability data performed at ambient temperature; data included from ref¹⁰ for comparison. ^bND = not determined. ^cn = 1 only.

Initial Biodistribution Studies

Mouse biodistribution studies over the course of 24 hours (n = 4 each time point) were performed with [¹¹¹In(*p*-NO₂-Bn-neunpa)]⁻ and [¹¹¹In(*p*-NH₂-Bn-CHX-A''-DTPA)]²⁻ and the data are summarized in Table 4. Both In-complexes were rapidly excreted through the kidneys and activity cleared quickly from all other organs. Notably, uptake of [¹¹¹In(*p*-NO₂-Bn-neunpa)]⁻ in the intestines was significantly higher than for [¹¹¹In(*p*-NH₂-Bn-CHX-A''-DTPA)]²⁻ after 15 min (17.9 ± 5.5% ID/g vs 3.6 ± 1.6% ID/g) and 1 h (39.8 ± 2.9% ID/g vs 10.7 ± 1.4% ID/g). One explanation for the difference in intestine uptake is that the mono-anionic ¹¹¹In-neunpa complex is more lipophilic than the di-anionic ¹¹¹In-*p*-NH₂-Bn-CHX-A''-DTPA complex, as evinced by shifts in the radio-HPLC retention times (t_R = 12.9 min and 8.6 min, respectively) and the absolute logP values of each complex (-1.65 ± 0.04, and -3.85 ± 0.17, respectively), thus shifting the excretion of the radiotracer from renal to intestinal elimination because highly charged polar substances are generally eliminated via the kidneys while less hydrophilic compounds tend to be eliminated via the intestinal tract. Nonetheless, the remaining ¹¹¹In-complex in the intestines at 1 h was rapidly excreted by 4 h for both complexes, and the uptake in intestines of [¹¹¹In(*p*-NO₂-Bn-neunpa)]⁻ and [¹¹¹In(*p*-NH₂-Bn-CHX-A''-DTPA)]²⁻ were no longer statistically different (p > 0.05) at later time points (0.265 ± 0.206% ID/g vs 0.160 ± 0.047% ID/g, for 4 h; 0.216 ± 0.114% ID/g vs 0.129 ± 0.06% ID/g, for 24 h, respectively). It has been suggested that administration of an unstable ¹¹¹In-complex would result in demetalation of the complex *in vivo* and subsequent accumulation of transche-

Table 5. Chemical and *in vitro* characterization data of ¹¹¹In-neunpa -/- CHX-A''-DTPA-Trastuzumab radioimmunoconjugates

Immunoconjugate	Radiolabeling conditions and yield	Chelate/mAb	Specific activity (mCi/mg)	Immunoreactive fraction (%)	Serum stability over 5 days (%)
¹¹¹ In-neunpa-Trastuzumab	pH 6, r.t., 15 or 30 min, 92.6 %	5.5 ± 1.1	28.0	>99	94.7 %
¹¹¹ In-CHX-A''-DTPA-Trastuzumab	pH 6, r.t., 30 min, 91.6%	4.6 ± 0.7	20.8	>99	ND

0.023 ± 0.006% ID/g for liver; 0.029 ± 0.01% ID/g vs 0.032 ± 0.008% ID/g for spleen; 0.010 ± 0.006% ID/g vs 0.007 ± 0.002% ID/g for bone, at 24 h, respectively). Furthermore, [¹¹¹In(*p*-NO₂-Bn-neunpa)] had improved kidney clearance compared to [¹¹¹In(*p*-NH₂-Bn-CHX-A''-DTPA)]²⁻ at 24 h (0.077 ± 0.058% ID/g vs 0.301 ± 0.043% ID/g, respectively, *p* < 0.05). Although these initial biodistribution data appear promising it may be that the predicted -1 and -2 charge of the In-neunpa/-CHX-A''-DTPA complexes, respectively, at physiological pH, could be mediating the rapid elimination of the metal-complexes from the body; therefore, the In-complexes may not have ample opportunity to dissociate *in vivo* giving the appearance of a stable complex. In order to further scrutinize the *in vivo* stability of ¹¹¹In-neunpa and ¹¹¹In-CHX-A''-DTPA an immuno-conjugate should be prepared (*vide infra*) and accordingly, biodistribution of each complex can be monitored over the course of several days instead of hours.

Preparation of Bioconjugates and *In Vitro* Characterization

The promising radiolabeling efficiencies and *in vitro* kinetic inertness of [¹¹¹In(*p*-NO₂-Bn-neunpa)] provided motivation to prepare and test the radiolabeling properties, and *in vivo* behaviour of a H₄neunpa-bioconjugate. The HER2/*neu*-targeting antibody Trastuzumab was chosen as the biovector because it is well established to target HER2-expressing tumors such as the SKOV-3 ovarian cancer cell line. To provide a basis for comparison, the gold-standard CHX-A''-DTPA was also conjugated to Trastuzumab and tested in parallel in the radiolabeling and *in vivo* experiments.

The novel bifunctional chelator *p*-SCN-Bn-H₄neunpa **9** and gold-standard *p*-SCN-Bn-CHX-A''-DTPA were conjugated to Trastuzumab, by incubation at room temperature at 5:1 molar ratio of ligand to antibody under slightly basic conditions (pH 9.0).³⁴ Final immunoconjugates were purified by spin filtration and stored at -20°C until use. A radiometric isotopic dilution assay was employed to determine the number of accessible chelates per antibody; an average of 5.5 ± 1.1 H₄neunpa chelates per antibody and 4.6 ± 0.7 CHX-A''-DTPA chelates per antibody were conjugated to Trastuzumab.

Preliminary ¹¹¹In radiolabeling efficiency of H₄neunpa-Trastuzumab was tested at pH 5.0, 5.5, and 6.0 in NH₄OAc buffer (0.15 M) at RT, and the radiochemical yield (RCY) was

assessed at 15 min. Calculated RCYs after 15 min were 15.0, 84.4, 92.6% at pH 5.0, 5.5, or 6.0, respectively (Figure S11). RCY was also assessed after 90 min for pH 5.0 and 6.0 reactions; yields increased to 38% and remained constant at 92% for pH 5.0 and 6.0, respectively. These initial radiolabeling tests suggest an optimal radiolabeling pH of 6.0 for H₄neunpa-Trastuzumab, in order to generate ¹¹¹In-conjugates of high radiochemical yield (>90%) and purity in only 15 min at RT. This is in agreement with a solution equilibrium study, which reflects the maximum of the [In(neunpa)] species formed at pH 6 (see distribution diagram in Figure S7). The kinetic inertness of ¹¹¹In-neunpa-Trastuzumab was assessed in an *in vitro* human serum challenge assay at 37°C. Much like the unconjugated precursor, ¹¹¹In-neunpa-Trastuzumab was exceptionally inert to transchelation when incubated with human serum, with 95.0 ± 1.1, 96.0 ± 2.5, 94.7 ± 0.6, and 94.8 ± 1.6% of the ¹¹¹In-bioconjugate remaining intact after 1, 2, 5, and 7 days, respectively.

¹¹¹In-labeled Trastuzumab conjugates were then prepared for *in vivo* studies. Both immunoconjugates were radiolabeled with ¹¹¹In in NH₄OAc buffer (0.15 M, pH 6) for 30 min at RT (Table 5), resulting in exceptionally high radiochemical yields (>90%) and radiochemically pure products (>99% after spin purification) for both ¹¹¹In-neunpa-Trastuzumab and ¹¹¹In-CHX-A''-DTPA-Trastuzumab. Final specific activities were determined to be 28.0 and 20.8 mCi/mg (1036 and 770 MBq/mg) for ¹¹¹In-neunpa-Trastuzumab and ¹¹¹In-CHX-A''-DTPA-Trastuzumab, respectively. *In vitro* cellular binding assays with SKOV-3 cancer cells showed both ¹¹¹In-immunoconjugates absolutely reactive towards the tested cell line (>99% immunoreactivity). Both ¹¹¹In-immunoconjugates have thus the ability to still bind to HER2.

Biodistribution and SPECT/CT Imaging Studies

In order to compare directly the pharmacokinetics of ¹¹¹In-neunpa-Trastuzumab to ¹¹¹In-CHX-A''-DTPA-Trastuzumab *in vivo*, biodistribution and single photon emission computed tomography (SPECT) in conjunction with helical X-ray CT imaging experiments were performed on female mice bearing subcutaneous SKOV-3 ovarian cancer xenografts on the left shoulder. Either tracer was injected via the tail vein (~37 MBq, ~35 – 50 µg, in 200 µL saline), and after 1, 3, and 5

days ($n = 4$ per time point) the mice were imaged ($n = 2$, Figure 4) and sacrificed to collect organs and tumors to be counted on a calibrated γ -counter.

SPECT/CT overlays of $^{111}\text{In-CHX-A''-DTPA-Trastuzumab}$ and $^{111}\text{In-neunpa-Trastuzumab}$ immunoconjugates are shown in Figure 5 at 1, 3 and 5 days post injection. These images were corrected for decay to allow qualitative comparison for the two radiolabeled immunoconjugates. For $^{111}\text{In-CHX-A''-DTPA-Trastuzumab}$ and $^{111}\text{In-neunpa-Trastuzumab}$, day 1 images show significant activity in the blood, the heart, the spleen and the tumor. The activity in the blood, the heart and the spleen decreases over time. The $^{111}\text{In-CHX-A''-DTPA-Trastuzumab}$ shows a higher activity in the tumor at all three time points, giving highly localized activity to the tumor site. On the other hand, $^{111}\text{In-neunpa-Trastuzumab}$ shows a lower uptake of activity into the tumor at day one post injection. Over time, the activity in the tumor decreased to being barely visible after 5 days post injection. Activity in the tumors for the $^{111}\text{In-neunpa-Trastuzumab}$ is still present at day 3 and 5 post-injection but in order to be able to compare the two tracers, an appropriate scale bar was required to prevent

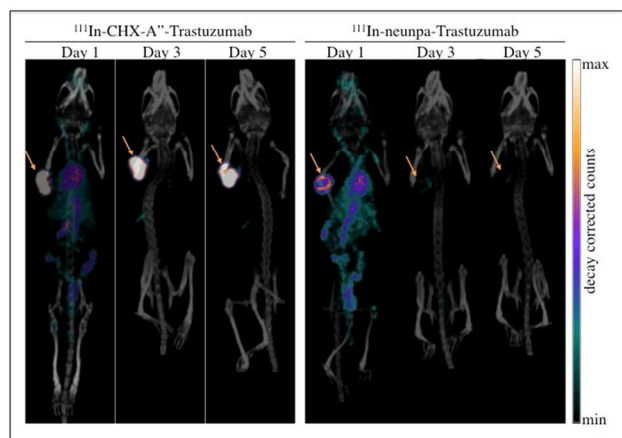


Figure 5. SPECT/CT overlays of $^{111}\text{In-CHX-A''-DTPA-Trastuzumab}$ (left) and $^{111}\text{In-neunpa-Trastuzumab}$ immunoconjugates. Fused $\mu\text{SPECT/CT}$ images in female mice with subcutaneous SKOV-3 xenografts on left shoulder, imaged at 1, 3 and 5 days post injection. Tumors are highlighted with arrows.

oversaturation of the high uptake of the $^{111}\text{In-CHX-A''-DTPA-Trastuzumab}$ within tumors. Reducing the max value of the scale bar by a factor of 2.8 shows the remaining activity within the tumors for the $^{111}\text{In-neunpa-Trastuzumab}$ (data not shown).

Comparing the biodistribution pattern of $^{111}\text{In-neunpa-Trastuzumab}$ with $^{111}\text{In-CHX-A''-DTPA-Trastuzumab}$, both tracer bioconjugates show the same general uptake profile, i.e. significant uptake in blood, spleen, liver, kidney, bone and tumor at day 1 (Figure 6 and Table S1). Three days and 5 days after immunoconjugate injection, the spleen and tumor still have the highest uptake of radiotracer compared to all other organs, but with significant difference ($p < 0.01$) between $^{111}\text{In-CHX-A''-DTPA-Trastuzumab}$ and $^{111}\text{In-neunpa-Trastuzumab}$ (49.65 \pm 6.79 %ID/g for $^{111}\text{In-CHX-A''-DTPA-Trastuzumab}$ and 21.47 \pm 6.61 %ID/g for $^{111}\text{In-neunpa-Trastuzumab}$ after 5 days in the spleen and 59.14 \pm 7.70 %ID/g for $^{111}\text{In-CHX-A''-DTPA-Trastuzumab}$ and 16.01 \pm 2.24 %ID/g for $^{111}\text{In-neunpa-Trastuzumab}$ after 5 days in the

tumor). This distribution of antibody-linked tracer is well known and is due to the metabolism and circulation of antibodies (or antibody-chelate conjugates).³⁵

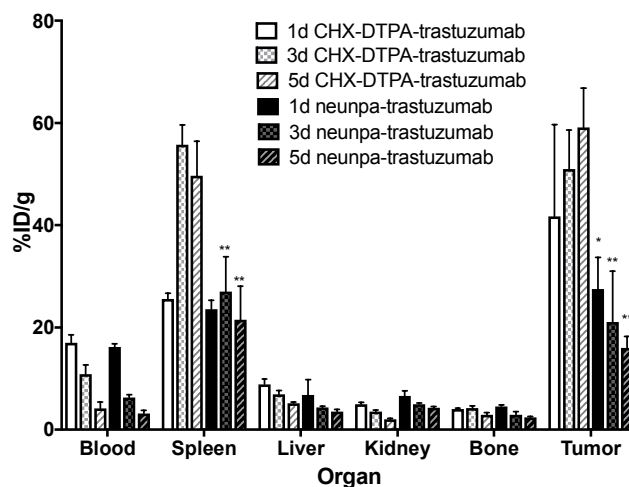


Figure 6. Biodistribution of $^{111}\text{In-CHX-A''-DTPA-Trastuzumab}$ compared to $^{111}\text{In-neunpa-Trastuzumab}$ in specific organs. Data are expressed as mean \pm SD ($n=4$). For statistical analysis * ($p \leq 0.05$) and ** ($p \leq 0.01$), two-way ANOVA.

The blood, liver, kidney and bone show the lowest %ID/g regarding all the different organs. The blood from $^{111}\text{In-neunpa-Trastuzumab}$ treated mice is cleared faster than the gold-standard $^{111}\text{In-CHX-A''-DTPA-Trastuzumab}$ between 1 d and 3 d. Additionally, $^{111}\text{In-CHX-A''-DTPA-Trastuzumab}$ shows an increase in accumulation in the tumor over time, whereas $^{111}\text{In-neunpa-Trastuzumab}$ shows a decrease of uptake into the tumor over time, which is consistent with the SPECT/CT overlay observations. Regarding the tumor:organ ratios (Figure 7), $^{111}\text{In-neunpa-Trastuzumab}$ and $^{111}\text{In-CHX-A''-DTPA-Trastuzumab}$ show interestingly only significant different values 5 d after injection for each ratio, tumor: blood, tumor: heart and tumor: muscle. Furthermore, the addition of the several chelating ligands onto Trastuzumab ($5.5 \pm 1.1 \text{ H}_4\text{neunpa}$ chelates per antibody and $4.6 \pm 0.7 \text{ CHX-A''-DTPA}$ chelates per antibody) can modify the overall charge of the antibody. Specifically, one negative charge per $[\text{In}(\text{neunpa})]^{3+}$ complex and two negative charges per $[\text{In}(\text{CHX-A''-DTPA})]^{2+}$ complex labeled to Trastuzumab is generated; this induces a two-fold increase of negative charge on the CHX-A''-DTPA-Trastuzumab conjugates compared to neunpa-Trastuzumab conjugates, assuming an equal number of accessible chelates are occupied by In^{3+} in each immunoconjugate. Consequently, this variance in overall charge of the Trastuzumab conjugate might affect the biodistribution of the resultant ^{111}In -tracer. The immunoreactivity results are comparable for H_4neunpa - and CHX-A''-DTPA-Trastuzumab conjugates, showing that the reactivity between Trastuzumab and its receptor is not altered due to the structural modification post chelate-conjugation. We wonder if the stability of the Trastuzumab-receptor-complex might not be as stable because of the charge difference discussed before. This could lead to a decreased uptake into the cancer cells. To conclude from these observations, different pharmacokinetic mechanisms for $^{111}\text{In-neunpa-Trastuzumab}$ and $^{111}\text{In-CHX-A''-DTPA-Trastuzumab}$ might

take place after 5 days. These differences will be investigated further in order to fully understand the mechanism of tumor uptake.

The slightly inferior uptake for this radiometal-neunpa antibody conjugate is disappointing but the complete chemistry and biology results suggest strongly that H₄neunpa is an attractive chelating ligand with a built In conjugatable moiety and should be investigated further with Bi³⁺ and in other In³⁺-biovector conjugates.

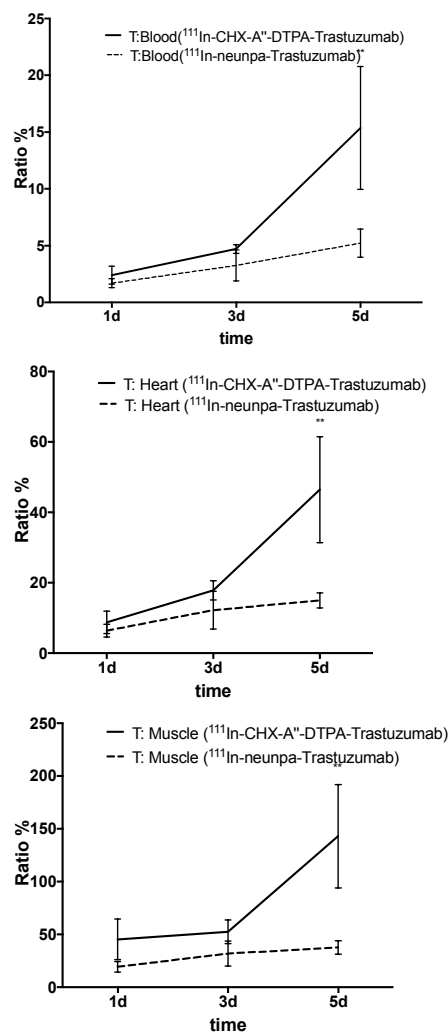


Figure 7. Tumor:Organ ratios of CHX-A''-DTPA and neunpa. Data is expressed as mean \pm SD (n=4). For statistical analysis ** ($p \leq 0.01$), two-way ANOVA.

Summary

The acyclic chelator *p*-NO₂-Bn-H₄neunpa and the bioconjugated analogue H₄neunpa-Trastuzumab (5.5 \pm 1.1 chelates per antibody) have been synthesized, characterized (HR-ESI-MS, ¹H NMR, ¹³C NMR, 2D-HSQC and cold metal complexation studies) and evaluated via radiolabeling with ¹¹¹In and ¹⁷⁷Lu. Unfortunately, low radiochemical yields of *p*-NO₂-Bn-H₄neunpa with ¹⁷⁷Lu were obtained (pH 4-5.5, ambient – 40°C, max. RCY 12.4 %). The radiolabeling yields of *p*-NO₂-Bn-H₄neunpa and H₄neunpa-Trastuzumab with ¹¹¹In were a

great success, >99 % and 92.6 %, respectively. Human serum stability experiments revealed that the [¹¹¹In(*p*-NO₂-Bn-neunpa)] complex and ¹¹¹In-neunpa-Trastuzumab immunoconjugate were 97.8 and 94.7 % intact after 5 days, respectively. H₄neunpa-Trastuzumab was highly immunoreactive (>99 %) as indicated by a cellular binding assay. Biodistribution study of [¹¹¹In(*p*-NO₂-Bn-neunpa)] in mice showed higher uptake into the intestine within the first hours compared to [¹¹¹In(CHX-A''-DTPA)]²⁻ due to its higher lipophilicity. Small animal SPECT/CT imaging and biodistribution studies of ¹¹¹In-neunpa-Trastuzumab were performed using female NOD.Cg-Prkdc^{scid} Il2rg^{tm1Wjl}/SzJ mice bearing SKOV-3 xenografts, and it was found that ¹¹¹In-neunpa-Trastuzumab successfully identified the tumor from surrounding tissues and other organs. Compared to the gold-standard ¹¹¹In-CHX-A''-DTPA-Trastuzumab, our immunoconjugate showed slightly lower tumor uptake which decreased over time and a lower tumor:blood ratio after 5 days post injection, although high quality SPECT/CT images were obtained. A different pharmacokinetic behavior of both immunoconjugates can be the result of different charges on the immunoconjugates. Thermodynamic stability experiments support these findings, since *p*-NO₂-Bn-H₄neunpa was found to bind strongly to large, highly charged metal ions like In³⁺, La³⁺ and Bi³⁺. Indeed, these results suggest H₄neunpa as a strong Bi(III) chelator and, considering the higher 3.6 units pM value respect to its In(III) complex, it could be of interest for Bi(III) isotopes (²¹²Bi and ²¹³Bi) in targeted alpha therapy (TAT). These encouraging results suggest H₄neunpa and its immunoconjugate have promise for studies with other radiometals and targeting vectors. These experiments are currently underway.

Experimental

Materials and Methods

All solvents and reagents were from commercial sources (Sigma Aldrich, TCI) and were used as received unless otherwise noted. *p*-NH₂-Bn-CHX-A''-DTPA and *p*-SCN-Bn-CHX-A''-DTPA were purchased from Macrocyclics (Dallas, TX) and used as received. Human serum was purchased frozen from Sigma Aldrich. ¹H and ¹³C NMR spectra were recorded at room temperature on a Bruker AV400 instrument; the NMR spectra are expressed on the δ (ppm) scale and are referenced to the residual solvent signal of the deuterated solvent. All spectra were recorded with sweep widths of 0-14 ppm or -20-220 ppm for ¹H and ¹³C NMR, respectively, and deviations in the presented spectra are magnifications for visualization purpose only. Assignments of the peaks in the NMR spectra are approximate. Mass spectrometry was performed on a Waters ZQ spectrometer equipped with an electrospray source. The HPLC system used for purification of ligands and precursors consisted of a Waters 600 controller equipped with a Waters 2487 dual λ absorbance detector connected to a Phenomenex synergi hydro-RP 80Å 250mm x 21.1 mm semi-preparative column. Analysis of ¹¹¹In and ¹⁷⁷Lu radiolabeled chelate complexes was carried out using a Phenomenex Synergi 4 μ Hydro-RP 80 Å analytical column (250 mm x 4.60 mm 4 μ m) using an Agilent HPLC system equipped with a model 1200 quaternary pump, a model 1200 UV absorbance detector (set at 250 nm), and a Raytest Gabi Star NaI(Tl) detector. The radiochemical purity and specific activity of the final ¹¹¹In radioimmunoconjugates was determined by using a size-exclusion chromatography (SEC) column (Phenomenex,

BioSep-SEC-s-3000) on an Agilent HPLC system equipped with a model 1200 quaternary pump, a model 1200 UV absorbance detector (set at 280 nm), and a Bioscan (Washington, DC) NaI scintillation detector (the radiodetector was connected to a Bioscan B-FC-1000 flow-count system, and the output from the Bioscan flow-count system was fed into an Agilent 35900E interface, which converted the analog signal to a digital signal). Instant thin layer chromatography paper strips impregnated with silica gel (iTLC-SG, Varian) were used to analyze crude ¹¹¹In-immunoconjugate labeling reactions and complex stability and counted on either a BioScan System 200 imaging scanner equipped with a BioScan Autochanger 1000 or on a Raytest miniGita with Beta GMC detector radio-TLC plate reader using TLC control Mini Ginastar software. PD-10 desalting columns (Sephadex G-25 M, 50 kDa, GE Healthcare) and centrifugal filter units with a 50 kDa molecular weight cutoff (Ultracel-50: regenerated cellulose, Amicon Ultra 4 Centrifugal Filtration Units, Millipore Corp.) were used for purification and concentration of antibody conjugates.

¹¹¹InCl₃ was cyclotron produced and provided by Nordion as a ~ 0.05 M HCl solution. ¹¹⁷LuCl₃ was purchased from Perkin-Elmer and provided as a solution in dilute HCl.

N,N-(2-Nitrobenzenesulfonamide)-1,2-triaminodiethane, **1**

Diethylenetriamine (4.19 mL, 38.8 mmol) was dissolved in THF (240 mL) and cooled to 0°C. Sodium carbonate Na₂CO₃ (9.04 g, 2.2 eq.) was added, followed by a slow addition of 2-nitrobenzenesulfonyl chloride (18.9 g, 85.3 mmol, 2.2 eq.), causing the reaction mixture to turn pale yellow. The reaction mixture was stirred overnight at room temperature. The off-white mixture was filtered to remove sodium carbonate and the filtrate was rotary evaporated to dryness. The crude product was purified by silica chromatography (CombiFlash Rf automated column system 220 g HP silica; solid (pause) preparation; A: hexanes, B: ethyl acetate, C: methanol, 100 % A to 100 % B gradient followed by 100 % C) to yield the product **1** as a yellow-orange solid (88 %, 16.15 g). ¹H NMR (400 MHz, acetone-d₆, 25°C): 8.13-8.11 (m, 2H), 7.94-7.89 (m, 6H), 3.11 (t, J = 7.32 Hz, 4H), 2.67 (t, J = 5.80 Hz, 4H). ¹³C NMR (101 MHz, acetone-d₆, 25°C): 134.0, 132.7, 130.7, 125.0, 47.7, and 43.1. HR-ESI-MS calcd. for [C₁₆H₁₉N₃O₈S₂+H]⁺: 474.0753; found 474.0749 [M+H]⁺.

N,N-(((4-Nitrophenyl)azanediyl)bis(ethane-2,1-diyl))bis(2-nitrobenzenesulfonamide), **2**

To a solution of **1** (16.15 g, 34.1 mmol) in DMF (60 mL) was added K₂CO₃ (6.13 g, 44.3 mmol, 1.3 eq.) and 4-(2-bromoethyl)nitrobenzene (10.20 g, 44.3 mmol, 1.3 eq.). After stirring the reaction mixture for 3 days at 40°C, the bright yellow solution was cooled to room temperature and the excess K₂CO₃ was removed by centrifugation. After drying the solution in vacuo, the crude dark red product was purified by silica chromatography (Combi Flash Rf automated column system; 80 g HP silica; solid (pause) preparation; A: hexane, B: ethyl acetate, 100% A to 100% B gradient) to yield product **2** as an orange fluffy solid (64.0 %, 13.59 g). ¹H NMR (400 MHz, CDCl₃, 25°C): 8.11-8.09 (d, J = 8.58 Hz, 2H), 8.08-8.06 (m, 2H), 7.84-7.81 (m, 2H), 7.76-7.73 (m, 4H), 7.32-7.30 (d, d = 8.58 Hz, 2H), 5.68 (s, 2H, NH), 3.07-3.05 (t, d = 5.63, 4H), 2.86-2.82 (t, J = 6.88, 2H), 2.74-2.72 (m, 2H), 2.70-2.67 (t, J =

6.62 Hz, 4H). ¹³C NMR (101 MHz, CDCl₃, 25°C): 158.0, 157.6, 147.5, 146.8, 129.6, 129.5, 124.0, 117.3, 114.4, 55.0, 52.5, 37.6, and 33.5. HR-ESI-MS calcd. for [C₂₄H₂₆N₆O₁₀S₂+H]⁺: 623.1230; found 623.1237 [M+H]⁺.

Dimethyl-6,6-((((4-nitrophenethyl)azanediyl)bis(ethane-2,1-diyl))bis(((2-nitrophenyl)sulfonyl)azanediyl))bis(methylene)-dipicolinate, **3**

To a solution of **2** (13.59 g, 21.8 mmol) in dry DMF (80 mL) was added methyl-6-bromomethyl picolinate (11.55 g, 50.2 mmol, 2.3 eq) and sodium carbonate (5.32 g, 50.2 mmol, 2.3 eq). The bright orange reaction mixture was stirred at 60°C overnight, filtered to remove excess sodium carbonate, and concentrated in vacuo. The crude product was purified by silica chromatography (CombiFlash Rf automated column system; 2 x 80 g silica; solid (pause) preparation; A: hexane, B: ethyl acetate, 100% A to 100% B gradient) to yield product **3** as an orange/brown oil (70 %, 14 g). ¹H NMR (400 MHz, CDCl₃, 25°C): 8.02-8.00 (m, 4H), 7.96 (d, J = 7.7 Hz, 2H), 7.78 (t, J = 7.8 Hz, 2H), 7.67-7.60 (m, 6H), 7.54 (d, J = 7.8 Hz, 2H), 7.18 (d, J = 8.4 Hz, 2H), 4.67 (s, 4H), 3.89 (s, 6H), 3.29 (t, J = 6.8 Hz, 4H), 2.58-2.51 (m, 8H). ¹³C NMR (101 MHz, CDCl₃, 25°C): 165.3, 157.0, 148.1, 147.6, 146.4, 138.1, 132.1, 129.7, 126.0, 125.9, 124.4, 124.4, 123.5, 55.3, 53.9, 52.9, 52.7, 46.9, and 33.4. HR-ESI-MS calcd. for [C₄₀H₄₀N₈O₁₄S₂+H]⁺: 921.2184; found 921.2184 [M+H]⁺.

Dimethyl-6,6-((((4-nitrophenethyl)azanediyl)bis(ethane-2,1-diyl)bis(azanediyl))bis(methylene)dipicolinate, **4**

To a solution of **3** (7.48 g, 8.1 mmol) in dry THF (100 mL) was added thiophenol (1.91 mL, 18.7 mmol, 2.3 eq.) and potassium carbonate (3.71g, 26.8 mmol, 3.3 eq.). The reaction mixture was stirred at 50°C for 72 hours, changing color to light orange. The excess salts were removed by centrifugation (5 min, 4000 rpm) followed by several washes with DMF. The filtrate was concentrated in vacuo in a (maximum) 50°C waterbath temperature. The resulting crude dark orange oil was purified by neutral alumina chromatography (CombiFlash Rf automated column system; 6 x 40 g neutral alumina; liquid injection A: dichloromethane, B: methanol, 100 % A to 20 % B gradient) to yield product **4** as an orange oil (32.4 %, 1.45 g). ¹H NMR (400 MHz, CDCl₃, 25°C): 8.01 (d, J = 8.6 Hz, 2H), 7.90 (d, J = 7.6 Hz, 2H), 7.73 (t, J = 7.8 Hz, 2H), 7.45 (d, J = 7.7 Hz, 2H), 7.28 (d, J = 8.6 Hz, 2H), 3.99 (s, 4H), 3.91 (s, 6H), 2.79-2.72 (m, 12H). ¹³C NMR (101 MHz, CDCl₃, 25°C): 165.6, 158.9, 148.6, 147.4, 164.4, 137.8, 129.7, 126.0, 123.9, 123.7, 55.9, 54.0, 53.0, 52.7, 47.0, and 33.3. HR-ESI-MS calcd. for [C₂₈H₃₄N₆O₆+H]⁺: 551.2618; found 551.2617 [M+H]⁺.

N,N-[(tert-Butoxycarbonyl)methyl-N,N-[6(methoxycarbonyl)pyridine-2-yl]methyl]-N-(4-nitrophenethyl)-1,2-triaminodiethane, **5**

To a solution of **4** (1.45 g, 2.6 mmol) in acetonitrile (60 mL) was added tert-butylbromoacetate (894 μL, 6.1 mmol, 2.3 eq.) and sodium carbonate (642 mg, 6.1 mmol, 2.3 eq.). The reaction mixture was stirred at 60°C overnight, filtered to remove excess sodium carbonate and concentrated in vacuo. The crude product was purified by silica chromatography (CombiFlash Rf automated system; 40g HP silica; A: dichloromethane, B: methanol, 100% A to 20% B gradient) to yield

product **5** as an orange oil (72 %, 1.48 g). ¹H NMR (400 MHz, CDCl₃, 25°C): 8.11 (d, J = 8.5 Hz, 2H), 8.03 (d, J = 7.7 Hz, 2H), 7.89 (t, J = 7.7 Hz, 2H), 7.52 (d, J = 7.6 Hz, 2H), 7.43 (d, J = 8.5 Hz, 2H), 4.18 (s, 4H), 3.96 (s, 6H), 3.90 (s, 4H), 3.73 (m, 2H), 3.54 (s, 4H), 3.45 (br s, 4H), 3.24 (m, 2H), 1.38 (s, 18H). ¹³C NMR (101 MHz, CDCl₃, 25°C): 168.7, 165.1, 156.7, 147.3, 147.3, 143.8, 139.1, 130.1, 127.5, 125.0, 124.0, 83.2, 57.5, 56.0, 54.5, 53.3, 50.4, 48.8, 29.8, 28.0. HR-ESI-MS calcd. for [C₄₀H₅₄N₆O₁₀H]⁺: 779.3980; found 779.3973 [M+H]⁺.

p-NO₂-Bn-H₄neunpa · 2.2 HCl · 3.1 H₂O, **6**

To compound **5** (0.23 g, 0.3 mmol) in THF/H₂O (3 mL, 3:1) was added lithium hydroxide (0.07 g, 3.0 mmol, 10 eq.) and the mixture was stirred for 16 h at room temperature. Solvents were evaporated and the crude product was purified by semi-preparative reverse-phase (RP) HPLC (10mL/ min, gradient A: 0.1% TFA in deionized water, B: acetonitrile, A: 95% to B: 100% for 25 min., t_R = 14.00 min) and the product **6** was obtained as a yellow oil (61 %, 0.12 g). ¹H NMR (400 MHz, CDCl₃, 25°C): 8.11 (d, J = 8.5 Hz, 2H), 8.03 (d, J = 7.7 Hz, 2H), 7.89 (t, J = 7.7 Hz, 2H), 7.52 (d, J = 7.6 Hz, 2H), 7.43 (d, J = 8.5 Hz, 2H), 4.18 (s, 4H), 3.90 (s, 4H), 3.73 (m, 2H), 3.54 (s, 4H), 3.45 (br s, 4H), 3.24 (m, 2H). ¹³C NMR (101 MHz, CDCl₃, 25°C): 168.7, 165.1, 156.7, 147.3, 147.3, 143.8, 139.1, 130.1, 127.5, 125.0, 124.0, 57.5, 56.0, 54.5, 48.8. HR-ESI-MS calcd. for [C₃₀H₃₄N₆O₁₀+H]⁺: 639.2415; found 639.2415 [M+H]⁺. Elemental analysis: calcd % for *p*-NO₂-Bn-H₄neunpa · 2.2 HCl · 3.1 H₂O: C 46.55 N 10.86 H 5.2; found: C 46.72, N 10.64, H 5.37.

N,N-[(tert-Butoxycarbonyl)methyl-N,N-[6(methoxycarbonyl)pyridine-2-yl]methyl]-N-(4-aminophenethyl)-1,2-triaminodiethane, **7**

Compound **5** (0.11 g, 0.1 mmol) was dissolved in glacial acetic acid (3 mL) and Pd/C 10% was added, the vessel sealed and purged with H₂ gas, charged with a H₂ balloon and left to stir for 2 h at room temperature. The reaction mixture was then filtered through Celite and concentrated under reduced pressure to yield compound **7**. The aromatic amine was confirmed by a purple ninhydrin staining. The solution was filtered and the filtrate was concentrated in vacuo. ¹H NMR (400 MHz, MeOD, 25°C): 7.99 (m, 2H), 7.92 (t, J = 7.9 Hz, 2H), 7.62 (d, J = 7.7 Hz, 2H), 6.87 (d, J = 7.9 Hz, 2H), 4.01 (s, 2H), 3.46 (br.4, 2H), 3.13 (m, 4H), 2.79 (m, 4H), 1.41 (s, 18H). ¹³C NMR (400 MHz, MeOD): 172.3, 166.7, 160.8, 148.3, 139.7, 139.5, 130.4, 128.3, 125.4, 125.2, 116.8, 82.7, 59.4, 56.9, 53.4, 52.3, 50.6, 29.9, 28.4. HR-ESI-MS calcd. for [C₄₀H₅₆N₆O₈+H]⁺: 749.4238; found 749.4236 [M+H]⁺.

p-NH₂-Bn-H₄neunpa, **8**

Compound **6** (0.09 g, 0.13 mmol) was dissolved in THF/H₂O (3 mL, 3:1) and lithium hydroxide (0.03 g, 1.26 mmol, 10 eq.) was added. The reaction mixture was left at room temperature for 24 hours. After product formation was confirmed by ESI-MS analysis, the solution was neutralized with 1 M HCl and solvents were concentrated *in vacuo*. For purification, semi-preparative RP-HPLC (10mL/ min, gradient A: 0.1% TFA in deionized water, B: acetonitrile, A: 95% to B: 100% for 25 min., t_R = 11.50 min) was used and product **8** was obtained as a yellow oil (50 %, 0.04 g). ¹H NMR (400 MHz, MeOD, 25°C):

8.05-8.04 (d, J = 6.6 Hz, 2H), 7.96-7.94 (d, J = 5.8 Hz, 2H), 7.63-7.61 (d, J = 6.6 Hz, 2H), 7.42-7.40 (d, J = 5.8 Hz, 2H), 7.32 (s, 2H), 4.08 (s, 4H), 3.71 (s, 4H), 3.59 (s, 2H), 3.53 (s, 4H), 3.35 (s, 4H), 3.14 (m, 2H). ¹³C NMR (400 MHz, MeOD): 173.5, 167.4, 159.0, 148.7, 140.3, 139.1, 131.8, 128.3, 125.6, 124.4, 116.7, 58.7, 56.5, 55.8, 53.1, 50.1, 30.4; ¹³C-DEPT NMR (400 MHz, MeOD): 140.3↑, 131.5↑, 128.1↑, 125.6↑, 124.2↑, 58.4↓, 56.4↓, 55.5↓, 51.5↓, 49.9↓, 30.2↓. HR-ESI-MS calcd. for [C₃₀H₃₇N₆O₈+H]⁺: 609.2673; found 609.2671 [M+H]⁺.

p-SCN-Bn-H₄neunpa, **9**

Compound **8** (0.04 g, 0.1 mmol) was dissolved in 0.1 M HCl (1 mL) and dichloromethane (1 mL). Thiophosgene (0.05 mL, 0.6 mmol, 10 eq) was added and the solution was stirred vigorously at room temperature overnight in the dark. The solvents were concentrated in vacuo and the product purified by semi-preparative RP-HPLC (10mL/ min, gradient A: 0.1% TFA in deionized water, B: acetonitrile, A: 95% to B: 100% for 25 min., t_R = 17.00 min) to yield product **9** as an orange oil (59 %, 0.02 g). ¹H NMR (400 MHz, MeOD, 25°C): 8.04-8.02 (d, J = 6.7 Hz, 2H), 7.95-7.92 (t, J = 8.2 Hz, 2H), 7.61-7.57 (t, J = 7.5 Hz, 2H), 7.27-7.25 (d, J = 7.5 Hz, 2H), 7.18-7.16 (d, J = 7.5 Hz, 2H), 4.05 (s, 4H), 3.66 (s, 4H), 3.55 (s, 2H), 3.50 (s, 4H), 3.26 (br s, 4H), 3.07 (m, 2H). ¹³C NMR (400 MHz, MeOD): 173.5, 167.4, 159.0, 148.7, 140.3, 137.5, 131.5, 128.3, 126.9, 125.6, 115.9, 58.7, 56.5, 55.8, 51.9, 50.1, 30.5; ¹³C-DEPT NMR (400 MHz, MeOD): 140.3↑, 131.4↑, 128.3↑, 126.9↑, 125.6↑, 58.7↓, 56.35↓, 56.5↓, 51.9↓, 50.1↓, 30.5↓. HR-ESI-MS calcd. for [C₃₁H₃₅N₆O₈+H]⁺: 651.2237; found 651.2239 [M+H]⁺.

Na[La(*p*-NO₂-Bn-neunpa)]

Compound **6** (10.2 mg, 16.0 mmol) was dissolved in water and lanthanum perchlorate (7.7 mg, 17.6 mmol, 1.1 eq.) was added. The pH was adjusted to 4 using 0.1 M NaOH. The successful La-complexation as a white precipitate was confirmed by HR-ESI-MS immediately after adding La(ClO₄)₄. After centrifugation, the precipitate was washed with water. ¹H NMR (400 MHz, DMSO-d₆, 25°C): 8.15 (d, 2H), 8.01 (m, 2H), 7.92 (m, 2H), 7.61 (d, J = 7.6 Hz, 2H), 7.50 (d, J = 8.5 Hz, 2H), 4.01 (s, 4H), 3.69 (m, 5H), 3.51 (d, 4H), 3.25 (s, 7H). HSQC (400 MHz, DMSO-d₆, 25°C) in Supporting Information. HR-ESI-MS calcd. for [C₃₀H₃₂N₆O₁₀La]⁺: 775.1243; found 775.1236 [M+2H]⁺.

Na[Bi(*p*-NO₂-Bn-neunpa)]

Compound **6** (20.3 mg, 31.8 mmol) was dissolved in water and bismuth trichloride (11.0 mg, 35.0 mmol, 1.1 eq.) was added. The pH was adjusted to 4 using 0.1 M NaOH. The successful Bi-complexation as a white precipitate was confirmed by HR-ESI-MS immediately after adding BiCl₃. After centrifugation, the precipitate was washed with water. The Bi-complex is not soluble in any solvent; DMSO-d₆ was chosen for NMR analysis. ¹H NMR and ¹³C NMR not measurable due to solubility problems. HR-ESI-MS calcd. for [C₃₀H₃₀N₆O₁₀Bi]⁺: 843.1827; found 843.1835 [M+2H]⁺.

Na[In(*p*-NO₂-Bn-neunpa)]

In a 20 mL screw cap vial, compound **6** (12 mg, 0.019 mmol) was dissolved in H₂O:MeOH (2:1, 1.5 mL). In a separate screw cap vial, [In(ClO₄)₃]·8H₂O (32 mg) was dissolved in dist. water (0.5 mL) to make a stock solution (64 mg/mL). An aliquot (217 μL, 13.8 mg, 0.0249 mmol) of this In(III) stock solution was added to the chelate solution. The pH of the solution was adjusted from pH 1 to pH 5 using 1 N NaOH and 0.1 M HCl. A stir bar was added, the reaction heated to 60°C in a sand bath and stirred for 3 hours with the lid loosely on. The mixture was removed from the heat and allowed to cool to room temperature. A white precipitate had formed, and the solution was then centrifuged and washed with dist. water (5 x 1 mL). After drying under high vacuum, the product as a white solid was collected (4 mg, 0.0053 mmol) with an overall yield of 28%. ¹H, and COSY NMR (400 MHz, DMSO-d₆) potential multiple isomers in solutions, see Figure S12 Supporting Information. HR-ESI-MS calculated for [¹¹⁵InC₃₀H₃₀N₆O₁₀+H+Na]⁺: 773.1038; found: 773.1039 (M+H+Na)⁺.

Bioconjugation of *p*-SCN-Bn-H₄neunpa and *p*-SCN-Bn-CHX-A''-DTPA to Trastuzumab.

Trastuzumab (Herceptin, Genentech, San Francisco, CA, USA) was purified using size exclusion columns (PD-10 desalting columns) and centrifugal filter units with a 50 kDa molecular weight cutoff and phosphate buffered saline (PBS, pH 7.4) to remove α-trehalose dehydrate, L-histidine, and polysorbate 20 additives. The purified antibody was brought up in PBS at pH 7.4. For each chelate-antibody conjugation, PBS (905 μL, pH adjusted to 9.0 using 0.1 M Na₂CO₃) and Trastuzumab (Genentech, San Francisco, CA, USA) (4 mg, 75 μL in PBS pH 7.4) was added to a low protein binding Eppendorf tube. To the antibody mixture, 5 equivalents of *p*-SCN-Bn-H₄neunpa or *p*-SCN-Bn-CHX-A''-DTPA was added, respectively, in small portions (5 x 5 μL in DMSO). The reaction mixture was stirred at ambient temperature overnight, and subsequently purified by centrifugal filtration. The final bioconjugates were stored in 0.25 M sodium acetate at -20°C. Final protein concentration was determined by the Bradford assay.

Chelate number – radiometric isotopic dilution assay.

The number of accessible chelating ligands conjugated per antibody was determined using previously described methods.^{36,37} Briefly, a 1 μCi/μL [¹¹¹In]InCl₃ working solution (non-radioactive In³⁺ spiked with ¹¹¹In) was prepared with a final In³⁺ concentration of 500 μM in ammonium acetate buffer (0.15 M, pH 6). In duplicate, for each chelate-antibody conjugate, 50 μg of bioconjugate (30 μL) was prepared into separate 1.5 mL Eppendorf tubes. Aliquots of 20, 25, and 30 μL of the [¹¹¹In]InCl₃ working solution were added to the two chelate-antibody samples. Positive controls containing 50 μg of bioconjugate and 25 μL of buffered ¹¹¹InCl₃ only (no non-radioactive In³⁺ added) were prepared in duplicate. Negative controls containing 30 μL of PBS, and 25 μL of [¹¹¹In]InCl₃ working solution were prepared in duplicate. Samples were allowed to incubate at room temperature overnight, after which time EDTA (50 mM, pH 5) was added at 1/9 of the reaction volume to scavenge any unspecifically bound In³⁺,

and incubated for 15 min. Each reaction mixture was spotted onto iTLC-SG plates, and developed using EDTA (50 mM, pH 5) as mobile phase. Radioactivity on the plate was measured using a radio-TLC plate reader, and number of chelates attached per antibody was calculated using equation (1).

$$nmol\ chelate = \frac{\# counts\ at\ baseline\ (R_f < 0.2)}{total\ \# counts} \times nmol\ In^{3+} \quad (1)$$

¹¹¹In-Chelate Radiolabeling Studies.

The ligand *p*-NO₂-Bn-H₄neunpa, or gold standard *p*-NH₂-Bn-CHX-A''-DTPA, was made up as a stock solution (1 mg/mL, ~10⁻³ M) in deionized water. From this stock solution, serial dilutions were prepared to final ligand concentrations of 10⁻⁴ M – 10⁻⁹ M. A 100 μL aliquot of each ligand stock (10⁻³ to 10⁻⁹ M) or water (blank control) was added to screw-cap mass spectrometry vials and diluted with sodium acetate buffer (pH 4, 10 mM, 880 μL). An aliquot of diluted ¹¹¹In stock (20 μL, ~200 μCi) was added to each vial and allowed to radiolabel at ambient temperature for 10 min, then it was analyzed by RP-HPLC to confirm radiolabeling and calculate yields. For human serum stability studies, undiluted ¹¹¹InCl₃ stock (~20 μL, 5 mCi) was added to the reaction vial containing 10⁻⁴ M ligand in sodium acetate buffer. Areas under the peaks observed in the HPLC radio-trace were integrated to determine radiolabeling yields. Elution conditions used for RP-HPLC analysis were gradient: A: 0.1% trifluoroacetic acid (TFA) in water, B: acetonitrile; 0 to 100% B linear gradient 20 min, 1 mL/min. [¹¹¹In(*p*-NO₂-Bn-neunpa)] (t_R = 12.9 min), [¹¹¹In(*p*-NH₂-Bn-CHX-A''-DTPA)]²⁻ (t_R = 8.0 min (minor product); 8.6 min (major product)) “¹¹¹In³⁺” (t_R = 5.3 min).

Partition Coefficients.

¹¹¹In-labeled complex (30 μL, 20 μCi) was diluted with phosphate buffered saline (pH 7.4, 470 μL), and added to 1-octanol (500 μL) in a 1.5 mL Eppendorf tube. Samples were vortexed for 60 seconds and subsequently centrifuged to separate phases (3000 rpm, 5 min). Aliquots (490 μL) of the aqueous and organic phases were diluted in a standard volume (20 mL) of water or acetonitrile, respectively, for measurement in an N-type Co-axial HPGe gamma spectrometer from Canberra fitted with a 0.5 mm beryllium window and calibrated (energy and efficiency) with a 20 mL ¹⁵²Eu and ¹³³Ba source. The samples were counted for a minimum of 5 minutes, with a dead time less than 5 %. The amount of ¹¹¹In-complex (Bq) in each fraction was quantified using the 171 and 245 keV gamma lines of ¹¹¹In.

¹¹¹In-neunpa/CHX-A''-DTPA-Trastuzumab Radiolabeling for *In Vivo* Studies.

Aliquots of H₄neunpa/CHX-A''-DTPA-Trastuzumab (650 μg) were diluted with ammonium acetate buffer (0.15 M, pH 6) such that the final volume of the reaction was 1 mL, and then ¹¹¹InCl₃ (~20 mCi) was added. The mixtures were allowed to react at ambient temperature for 40 min, and then analysed via iTLC-SG using 50 mM EDTA (pH 5) as eluent; ¹¹¹In-labelled antibody remained at the baseline, while ¹¹¹In³⁺ ions complexed as ¹¹¹In-EDTA and eluted with the solvent front. Radiolabeled immunoconjugates were then purified by PD-10 SEC columns and centrifugal filtration (50k cut-off). The radiochemical purity of the final radiolabeled bioconjugates was

determined using SEC-HPLC (using an isocratic gradient of 0.1 M sodium phosphate monobasic dehydrate, 0.1 M sodium phosphate dibasic dodecahydrate, 0.1 M sodium azide and 0.15 M sodium chloride (pH 6.2-7.0)); the specific activity was calculated by injecting a known activity, and integrating areas under the peaks of the UV-chromatogram measured against a standard curve.

In Vitro Human Serum Stability Data.

The procedures of the serum competition studies followed closely those previously published.^{8,10} The compound [¹¹¹In(*p*-NO₂-Bn-neunpa)]⁺, [¹¹¹In(*p*-NH₂-Bn-CHX-A⁺-DTPA)]²⁺, or blank control “¹¹¹In³⁺”, was prepared using the radiolabeling protocol as described above. In triplicate for the ¹¹¹In-complex, solutions were prepared in vials containing 330 μL of ¹¹¹In-complex (~1.6 mCi), 1000 μL of room temperature human serum, and 670 μL of phosphate buffered saline (PBS, pH 7.4) and incubated at 37°C. At time points of 1 h, 1 and 5 days, 400, 400, and 800 μL aliquots of the human serum competition mixture were removed from each vial, respectively, diluted to a total volume of 2.5 mL with PBS, and counted in a Capintec CRC-55r dose calibrator; this value is recorded as “full activity” to be loaded onto the PD-10 column. The 2.5 mL of reaction mixture was loaded onto a pre-conditioned PD-10 column, and the empty vial was counted again in the dose calibrator – this value was recorded as “residual activity” left in the vial. The loaded effluent was collected in a waste container, and then the PD-10 column was eluted with 3.5 mL of PBS, and collected into a separate vial. The eluent that contained ¹¹¹In bound/associated with serum proteins (size exclusion for MW < 5000 Da) was counted in the dose calibrator and then compared to the total activity that was loaded onto the PD-10 column to obtain the percentage of ¹¹¹In that was bound to serum proteins and therefore no longer chelate-bound by the relationship: 1 – (eluted activity/(full activity – residual activity)) x 100. For serum stability of the radioimmunoconjugates, ¹¹¹In-neunpa-Trastuzumab was first prepared as described above by incubating H₄neunpa-Trastuzumab (200 μg) and ¹¹¹InCl₃ (~1 mCi) in NH₄OAc (0.15 M, pH 6) for 20 minutes at ambient temperature. After confirming a radiolabeling yield >95% via iTLC-SG in 50 mM EDTA (pH 5), in triplicate, ¹¹¹In-neunpa-Trastuzumab (330 μL, ~320 μCi) was incubated with human serum (330 μL) and the mixture was left at 37°C for 168 h (7 d). At time points of 0, 1, 24, 48, 120, and 168 h, aliquots (3 – 5 μL) of the competition mixture was spotted on iTLC-SG plates and developed in 50 mM EDTA (pH 5) as described above.

Cell Culture.

The human ovarian adenocarcinoma HER2-positive SKOV-3 cells were cultured at 37°C with 5% CO₂ in Dulbecco's modified Eagle's medium (DMEM, LifeTechnologies, Rockford, IL, USA) containing 2 mM glutamine and supplemented with 10% fetal bovine serum (Sigma-Aldrich, Oakville, ON, USA) and 100 U/mL of penicillin-streptomycin (LifeTechnologies).

In Vitro Immunoreactivity Assay.

The immunoreactive fractions of ¹¹¹In-neunpa-Trastuzumab and ¹¹¹In-CHX-A⁺-DTPA-Trastuzumab were determined according to the Lindmo cell-binding method³⁸ using SKOV-3 cells^(37, 39) as previously described. Briefly, cells were sus-

pending at 0.23 to 2.3 x 10⁶ cells/mL in PBS (pH 7.4). For each tested antibody, 50 μL (from a solution of 0.45 μg of each radioimmunoconjugate diluted in 5 mL of 1% PBS-BSA) was added to each cell concentration tube in duplicate. The radio-labeled immunoconjugates were incubated for 1 h at 37 °C and under gentle agitation. Cells were then pelleted and washed twice with PBS. Each cell-bound activity for the different cell conditions was determined by measuring the ¹¹¹In amount of activity within the cell pellets using the Wallac WIZARD2 gamma counter with background and decay correction. The bound fraction was determined as a percentage of total added activity according to control samples. Immunoreactive fractions were estimated for conditions representing infinite antigen excess by linear regression analysis of a plot of total/bound activity against 1/[cell concentration]. Results >80% were considered suitable for *in vivo* imaging.

SKOV-3 Xenograft Mouse Models.

All experiments were conducted in accordance with the guidelines established by the Canadian Council on Animal Care and approved by the Animal Ethics Committee of the University of British Columbia (protocol # A16-0104). Female NOD.Cg-Prkdc^{scid} Il2rg^{tm1Wjl}/SzJ mice (4 months old) obtained from an in-house breeding colony were subcutaneously injected with 8 x 10⁶ SKOV-3 cells in matrigel (BD Bioscience) on the left flank.

[¹¹¹In(*p*-NO₂-Bn-neunpa)]⁺ and [¹¹¹In(*p*-NH₂-Bn-CHX-A⁺-DTPA)]²⁺ *in vivo* Biodistribution.

[¹¹¹In(*p*-NO₂-Bn-neunpa)]⁺ and [¹¹¹In(*p*-NH₂-Bn-CHX-A⁺-DTPA)]²⁺ were prepared according to the radiolabeling protocol above using 10⁻⁴ M ligand and ~ 148 MBq (~4 mCi) of ¹¹¹InCl₃ in sodium acetate buffer (10 mM, pH 4). Radiolabeling yields >99% were confirmed by RP-HPLC. Each radio-labeled tracer was diluted with PBS (pH 7.4) to a concentration of 10 MBq/mL (370 μCi/mL). Each mouse was intravenously injected through the tail vein with ~ 1 MBq (100 μL) of the ¹¹¹In complex and then sacrificed by inhalation of isoflurane followed by CO₂ at 15 min, 1 h, 4 h, or 24 h after injection (n = 4 at each time point). Blood was withdrawn by cardiac puncture and tissues of interest including fat, uterus, ovaries, intestine, spleen, liver, pancreas, stomach, adrenal glands, kidney, lungs, heart, muscle, bone (tibia), brain, and tail were harvested, washed in PBS, dried and weighed. Activity of each sample was measured by a calibrated gamma counter (Perkin Elmer, Wizard 2 2480) with decay correction. The activity uptake was expressed as a percentage of the injected dose per gram of tissue (%ID/g).

¹¹¹In-neunpa/CHX-A⁺-DTPA-Trastuzumab SPECT/CT Imaging and Biodistribution Studies.

Mice with SKOV-3 ovarian cancer xenografts were administered with ~37 MBq (~1 mCi) of ¹¹¹In-neunpa-trastuzumab (1.03 MBq/μg [28.0 μCi/μg]) or ¹¹¹In-CHX-A⁺-DTPA-Trastuzumab (0.77 MBq/μg [20.8 μCi/μg]) in ~30 μL of PBS (pH 7.4) via tail vein injection. For each radioimmunoconjugate, mice were imaged (n=2) at 1, 3, or 5 day after injection. Image acquisition and reconstruction was performed using the U-SPECT-II/CT (MILabs, Utrecht, The Netherlands). Approximately 5 min prior to SPECT/CT image acquisition, mice were anesthetized via inhalation of 2% isoflurane/oxygen gas

mixture and placed on the scanner bed. Anesthesia was maintained during imaging as well as body temperature via a heating pad. A 5 min baseline CT scan was obtained for localization with voltage setting at 60 kV and current at 615 μ A followed by a static emission scan using an ultra-high-resolution multi-pinhole rat-mouse (1 mm pinhole size) collimator. Data were acquired in list mode, reconstructed using the U-SPECT II software and co-registered for alignment. SPECT images were reconstructed using maximum-likelihood expectation maximization (3 iterations), pixel-based ordered subset expectation maximization (16 subsets) and a post-processing filter (Gaussian blurring) of 0.5 mm centered at photopeaks 171 keV and 245 keV with a 20% window width. Imaging data sets were decayed corrected to injection time and converted to DICOM data for visualization in the Inveon Research Workplace (Siemens Medical Solutions USA, Inc.). As no calibration factor was used or attenuation and scatter correction were performed on the images; they were used only for qualitative comparison between the two tracers and are presented using a min-max min-max scale bar of counts corrected for decay. For biodistribution studies, mice were sacrificed by inhalation of isoflurane followed by CO₂ (n = 4 at each time point), blood was withdrawn by cardiac puncture and tissues were collected and processed as described above. Tissues collected include all those listed above in addition to tumor tissue.

Solution Thermodynamics.

Protonation constants and metal stability constants were calculated from potentiometric titrations using a Metrohm Titrand 809 equipped with a Ross combined electrode and a Metrohm Dosino 800. The titration apparatus consisted of a 20 mL and 25 °C thermostated glass cell and an inlet-outlet tube for nitrogen gas (purified through a 10% NaOH solution) to exclude any CO₂ prior and during the course of the titration. The electrode was daily calibrated in hydrogen ion concentrations using a standard HCl as described before¹³ in order to obtain the calibration parameters E₀ and pK_w. Solutions were titrated with carbonate-free NaOH (0.157 M) that was standardized against freshly recrystallized potassium hydrogen phthalate. Protonation equilibria of the ligand were studied by titrations of a solution containing H₄neunpa 7.18 × 10⁻⁴ M at 25 °C and 0.16 M NaCl ionic strength using a combined potentiometric-spectrophotometric procedure.^{16,17} Spectra were recorded in the 200–450 nm spectral range with a 0.2 cm path length fiber optic on a Varian Cary 60 UV/Vis Spectrophotometer. In the study of complex formation equilibria, the ligand-metal solutions were prepared by adding the atomic absorption (AA) standard metal ion solutions to a H₄neunpa solution of known concentration in the 1:1 metal to ligand molar ratio. The exact amount of acid present in the lanthanum, bismuth and indium standards was determined by Gran's method⁴⁰ titrating equimolar solutions of either La(III), Bi(III) or In(III) and Na₂H₂-EDTA. Ligand and metal concentrations were in the range of 0.7-1.0 mM. Each titration consisted of 100-150 equilibrium points in the pH range 1.8-11.5, equilibration times for titrations were 2 min for pK_a titrations and up to 15 min for metal complex titrations. At least two replicate titrations were performed for each individual system. Potentiometric data were processed using the Hyperquad2013 software⁴¹ while the obtained spectrophotometric data were processed with the HypSpec.⁴¹ Proton dissociation constants corresponding to hydrolysis of La(III), Bi(III) and In(III) aqueous ions

and the indium-chloride stability constants included in the calculations were taken from Baes and Mesmer.⁴² The overall equilibrium (formation) constants log β are referred to the overall equilibria: pM + qH + rL = MpHpLr (the charges are omitted), where p might also be 0 in the case of protonation equilibria and q may be negative. Stepwise equilibrium constants log K correspond to the difference in log units between the overall constants of sequentially protonated (or hydroxide) species. The pM values for metal complexes were calculated by using the Hyss software⁴³, from the set of stability constants for each system at pH 7.4 with [L] = 1.0 × 10⁻⁵ M and [M] = 1.0 × 10⁻⁶ M.

Corresponding Author

*Email: orvig@chem.ubc.ca

ORCID Chris Orvig 0000-0002-2830-5493

Notes

The authors declare no competing financial interest.

Acknowledgments

Funding for this work was provided by the Canadian Institutes for Health Research (CIHR) and the Natural Sciences and Engineering Research Council (NSERC) of Canada as a Collaborative Health Research Project (CHRP). We acknowledge Nordion (Canada) for their in-kind contribution of ¹¹¹InCl₃. TRIUMF receives funding via a contribution agreement with the National Research Council of Canada. We would also like to thank Victoria Braun for helping conducting logP measurements.

Supporting Information

The Supporting Information is available free of charge on the ACS Publications website.

3D videos of ¹¹¹In-CHX-A''-DTPA-Trastuzumab and ¹¹¹In-neunpa-Trastuzumab can be found online under the following link:

<https://www.youtube.com/playlist?list=PLs31b0Z6H1z2CqUpljQrOh6vqtNAWBMYb>

Abbreviations

SPECT, single photon emission computed tomography; BFC, bifunctional chelator; DOTA, 1,4,7,10-tetraazacyclododecane-1,4,7,10-tetraacetic acid; DTPA, 2-[Bis[2-bis(carboxymethyl)amino]ethyl]amino]acetic acid; CHX, cyclohexyl; CN, coordination number, HER2/neu, human epidermal growth factor receptor 2; mAb, monoclonal antibody; CT, computed tomography.

References

- Holland, J. P., Williamson, M. J., and Lewis, J. S. (2010) Unconventional Nuclides for Radiopharmaceuticals, *Mol. Imaging* 9, 1-20.
- Price, E. W., and Orvig, C. (2014) Matching chelators to radiometals for radiopharmaceuticals, *Chem. Soc. Rev.* 43, 260-290.
- Tatsi, A., Maina, T., Cescato, R., Waser, B., Krenning, E. P., de Jong, M., Cordopatis, P., Reubi, J. C., and Nock, B. A. (2014)

[DOTA]Somatostatin-14 analogs and their (111)In-radioligands: effects of decreasing ring-size on sst1-5 profile, stability and tumor targeting, *Eur. J. Med. Chem.* **73**, 30-37.

4. Mojtahedi, A., Thamake, S., Tworowska, I., Ranganathan, D., and Delpassand, E. S. (2014) The value of (68)Ga-DOTATATE PET/CT in diagnosis and management of neuroendocrine tumors compared to current FDA approved imaging modalities: a review of literature, *Am. J. Nucl. Med. Mol. Imaging* **4**, 426-434.

5. Price, E. W., Cawthray, J. F., Adam, M. J., and Orvig, C. (2014) Modular syntheses of H(4)octapa and H(2)dedpa, and yttrium coordination chemistry relevant to ⁸⁶Y/⁹⁰Y radiopharmaceuticals, *Dalton Trans.* **43**, 7176-7190.

6. Price, E. W., Zeglis, B. M., Cawthray, J. F., Lewis, J. S., Adam, M. J., and Orvig, C. (2014) What a Difference a Carbon Makes: H₄octapa vs H₄C₃octapa, Ligands for In-111 and Lu-177 Radiochemistry, *Inorg. Chem.* **53**, 10412-10431.

7. Price, E. W., Zeglis, B. M., Lewis, J. S., Adam, M. J., and Orvig, C. (2014) H(6)phospa-Trastuzumab: Bifunctional Methylene phosphonate-based Chelator with ⁸⁹Zr, ¹¹¹In and ¹⁷⁷Lu, *Dalton Trans.* **43**, 119-131.

8. Ramogida, C. F., Cawthray, J. F., Boros, E., Ferreira, C. L., Patrick, B. O., Adam, M. J., and Orvig, C. (2015) H₂CHXdedpa and H₄CHXoctapa—Chiral Acyclic Chelating Ligands for ^{67/68}Ga and ¹¹¹In Radiopharmaceuticals, *Inorg. Chem.* **54**, 2017-2031.

9. Price, E. W., Zeglis, B. M., Cawthray, J. F., Ramogida, C. F., Ramos, N., Lewis, J. S., Adam, M. J., and Orvig, C. (2013) H₄octapa-Trastuzumab: Versatile Acyclic Chelate System for ¹¹¹In and ¹⁷⁷Lu Imaging and Therapy, *J. Am. Chem. Soc.* **135**, 12707-12721.

10. Price, E. W., Cawthray, J. F., Bailey, G. A., Ferreira, C. L., Boros, E., Adam, M. J., and Orvig, C. (2012) H₄octapa: An Acyclic Chelator for ¹¹¹In Radiopharmaceuticals, *J. Am. Chem. Soc.* **134**, 8670-8683.

11. Shannon, R. D. (1976) Revised effective ionic radii and systematic studies of interatomic distances in halides and chalcogenides, *Acta Crystallographica Section A* **32**, 751-767.

12. Arane, K. (2015) Synthesis and Characterization of H₅decapa and Related Ligand, in *Department of Inorganic Chemistry*, University of British Columbia.

13. Weekes, D. M., Ramogida, C. F., Jaraquemada-Peláez, M. d. G., Patrick, B. O., Apte, C., Kostelnik, T. I., Cawthray, J. F., Murphy, L., and Orvig, C. (2016) Dipicolinate Complexes of Gallium(III) and Lanthanum(III), *Inorg. Chem.* **55**, 12544-12558.

14. Montavon, G., Le Du, A., Champion, J., Rabung, T., and Morgenstern, A. (2012) DTPA complexation of bismuth in human blood serum, *Dalton Trans.* **41**, 8615-8623.

15. Burai, L., Fabian, I., Kiraly, R., Szilagyi, E., and Brucher, E. (1998) Equilibrium and kinetic studies on the formation of the lanthanide(III) complexes, [Ce(dota)]- and [Yb(dota)]-(H₄dota=1,4,7,10-tetraazacyclododecane-1,4,7,10-tetraacetic acid), *Dalton Trans.*, 243-248.

16. Nurchi, V. M., Crisponi, G., Crespo-Alonso, M., Lachowicz, J. I., Szweczuk, Z., and Cooper, G. J. S. (2013) Complex formation equilibria of CuII and ZnII with triethylenetetramine and its mono- and di-acetyl metabolites, *Dalton Trans.* **42**, 6161-6170.

17. Nurchi, V. M., Lachowicz, J. I., Crisponi, G., Murgia, S., Arca, M., Pintus, A., Gans, P., Niclos-Gutierrez, J., Dominguez-Martin, A., Castineiras, A., Remelli, M., Szweczuk, Z., and Lis, T. (2011) Kojic acid derivatives as powerful chelators for iron(III) and aluminium(III), *Dalton Trans.* **40**, 5984-5998.

18. Mato-Iglesias, M., Balogh, E., Platas-Iglesias, C., Toth, E., de Blas, A., and Rodriguez Blas, T. (2006) Pyridine and phosphonate containing ligands for stable lanthanide complexation. An experimental and theoretical study to assess the solution structure, *Dalton Trans.*, 5404-5415.

19. Kálmán, F. K., Végh, A., Regueiro-Figueroa, M., Tóth, É., Platas-Iglesias, C., and Tircsó, G. (2015) H₄octapa: Highly Stable Complexation of Lanthanide(III) Ions and Copper(II), *Inorg. Chem.* **54**, 2345-2356.

20. Moeller, T., and Thompson, L. (1962) Observations on the rare earths—LXXV (1): The stabilities of

diethylenetriaminepentaacetic acid chelates, *J. Inorg. Nucl. Chem.* **24**, 499-510.

21. Smith, R. M., Martell, A. E., Motekaitis, R. J., and Standard Reference Data, p. (2004) NIST critically selected stability constants of metal complexes database, Standard Reference Data Program, National Institute of Standards and Technology, U.S. Dept. of Commerce, Gaithersburg, MD.

22. Csajbók, É., Baranyai, Z., Bányai, I., Brücher, E., Király, R., Müller-Fahrnow, A., Platzek, J., Radüchel, B., and Schäfer, M. (2003) Equilibrium, ¹H and ¹³C NMR Spectroscopy, and X-ray Diffraction Studies on the Complexes Bi(DOTA)- and Bi(DO3A-Bu), *Inorg. Chem.* **42**, 2342-2349.

23. Gerald, C. F. G. C., Delgado, R., Urbano, A. M., Costa, J., Jasanada, F., and Nepveu, F. (1995) Complexes of Ga³⁺ and In³⁺ with the N₃N[double prime]-bis(butylamide) derivative of diethylenetriaminepentaacetic acid: stability constants and nuclear magnetic resonance studies in aqueous solution, *Dalton Trans.*, 327-335.

24. Martell, A. E., Smith, R. M. (1974-1989) *Critical Stability Constants*, Vol. 1-6, Plenum Press: New York.

25. Lima, L. M. P., Beyler, M., Delgado, R., Platas-Iglesias, C., and Tripier, R. (2015) Investigating the Complexation of the Pb²⁺/Bi³⁺ Pair with Dipicolinate Cyclen Ligands, *Inorg. Chem.* **54**, 7045-7057.

26. Ramogida, C. F., and Orvig, C. (2013) Tumour targeting with radiometals for diagnosis and therapy, *Chem. Comm.* **49**, 4720-4739.

27. Hosseinimehr, S. J., Orlova, A., and Tolmachev, V. (2010) Preparation and in vitro evaluation of ¹¹¹In-CHX-A"-DTPA-labeled anti-VEGF monoclonal antibody bevacizumab, *Hum. Antibodies* **19**, 107-111.

28. Massa, S., Vikani, N., Betti, C., Ballet, S., Vanderhaegen, S., Steyaert, J., Descamps, B., Vanhove, C., Bunschoten, A., et al (2016) Sortase A-mediated site-specific labeling of camelid single-domain antibody-fragments: a versatile strategy for multiple molecular imaging modalities, *Contrast Media Mol. Imaging* **11**, 328-339.

29. Shin, I. S., Lee, S. M., Kim, H. S., Yao, Z., Regino, C., Sato, N., Cheng, K. T., Hassan, R., Campo, M. F., Albone, E. F., et al (2011) Effect of chelator conjugation level and injection dose on tumor and organ uptake of ¹¹¹In-labeled MORAb-009, an anti-mesothelin antibody, *Nucl. Med. Biol.* **38**, 1119-1127.

30. Timmermand, O. V., Ulmert, D., Evans-Axelsson, S., Pettersson, K., Bjartell, A., Lilja, H., Strand, S.-E., and Tran, T. A. (2014) Preclinical imaging of kallikrein-related peptidase 2 (hK2) in prostate cancer with a ¹¹¹In-radiolabelled monoclonal antibody, 11B6, *EJNMMI Research* **4**, 51.

31. Tolmachev, V., Xu, H., Wällberg, H., Ahlgren, S., Hjertman, M., Sjöberg, A., Sandström, M., Abrahmsén, L., Brechbiel, M. W., and Orlova, A. (2008) Evaluation of a Maleimido Derivative of CHX-A" DTPA for Site-Specific Labeling of Affibody Molecules, *Bioconj. Chem.* **19**, 1579-1587.

32. Camera, L., Kinuya, S., Garmestani, K., Wu, C., Brechbiel, M. W., Pai, L. H., McMurry, T. J., Gansow, O. A., Pastan, I., Paik, C. H., and et al. (1994) Evaluation of the serum stability and in vivo biodistribution of CHX-DTPA and other ligands for yttrium labeling of monoclonal antibodies, *Journal of nuclear medicine : official publication, Society of Nuclear Medicine* **35**, 882-889.

33. Ando, A., Ando, I., Hiraki, T., and Hisada, K. (1989) Relation between the location of elements in the periodic table and various organ-uptake rates, *Nucl. Med. Biol.* **16**, 57-80.

34. Vosjan, M. J., Perk, L. R., Visser, G. W., Budde, M., Jurek, P., Kiefer, G. E., and van Dongen, G. A. (2010) Conjugation and radiolabeling of monoclonal antibodies with zirconium-89 for PET imaging using the bifunctional chelate p-isothiocyanatobenzyl-desferrioxamine, *Nat. Protoc.* **5**, 739-743.

35. Tabrizi, M., Bornstein, G. G., and Suria, H. (2010) Biodistribution mechanisms of therapeutic monoclonal antibodies in health and disease, *The AAPS journal* **12**, 33-43.

36. Meares, C. F., McCall, M. J., Reardan, D. T., Goodwin, D. A., Diamanti, C. I., and McTigue, M. (1984) Conjugation of antibodies with bifunctional chelating agents: isothiocyanate and

bromoacetamide reagents, methods of analysis, and subsequent addition of metal ions, *Anal. Biochem.* **142**, 68-78.

37. Deri, M. A., Ponnala, S., Kozlowski, P., Burton-Pye, B. P., Cicek, H. T., Hu, C., Lewis, J. S., and Francesconi, L. C. (2015) p-SCN-Bn-HOPO: A Superior Bifunctional Chelator for ^{89}Zr ImmunopET, *Bioconj. Chem.* **26**, 2579-2591.

38. Lindmo, T., Boven, E., Cuttitta, F., Fedorko, J., and Bunn, P. A., Jr. (1984) Determination of the immunoreactive fraction of radiolabeled monoclonal antibodies by linear extrapolation to binding at infinite antigen excess, *J. Immunol. Methods* **72**, 77-89.

39. Rousseau, J., Zhang, Z., Dias, G. M., Zhang, C., Colpo, N., Bénard, F., and Lin, K.-S. (2017) Design, synthesis and evaluation of

novel bifunctional tetrahydroxamate chelators for PET imaging of ^{89}Zr -labeled antibodies, *Bioorg. Med. Chem. Let.* **27**, 708-712.

40. Gran, G. (1952) Determination of the equivalence point in potentiometric titrations. Part II, *Analyst* **77**, 661-671.

41. Gans, P., Sabatini, A., and Vacca, A. (1996) Investigation of equilibria in solution. Determination of equilibrium constants with the HYPERQUAD suite of programs, *Talanta* **43**, 1739-1753.

42. Baes, C. F. J., and Mesmer, R. E. (1976) *The Hydrolysis of Cations*, Wiley, New York.

43. Alderighi, L., Gans, P., Ienco, A., Peters, D., Sabatini, A., and Vacca, A. (1999) Hyperquad simulation and speciation (HySS): a utility program for the investigation of equilibria involving soluble and partially soluble species, *Coord. Chem. Rev.* **184**, 311-318.

